High-temperature tribological investigations of CrAlN and CrAlSiN hard coatings in ambient and inert atmospheres

Ao Xia

Leoben, June, 2016

This work has been carried out at the Chair of Functional Materials and Materials Systems at the Department of Physical Metallurgy and Materials Testing, Montanuniversität Leoben, Austria.

Affidavit

I declare in lieu of oath, that I wrote this thesis and performed the associated research myself, using only literature cited in this volume.

Leoben, June, 2016

Acknowledgement

I would like to express my sincere gratitude to Univ. Prof. DI Dr.mont. Christian Mitterer, head of the Thin Film Group at the Department of Physical Metallurgy and Materials Testing, for the professional supervision and efforts he put in me. Thank you for the possibility of writing this thesis at your chair!

I am grateful to my supervisor Dr.mont. Marisa Rebelo De Figueiredo, for her scientific precision, quick responses to my questions, patience, good humor and exact corrections of this thesis. Thank you for your skilled guidance as a supervisor!

Furthermore I would like to express my gratitude to Dipl.-Phys. Dr.mont. Robert Franz, who acquainted me with LaTeX and also guided me through the thesis with his advice, patience and encouragement. Thank you for spending a lot of time in answering my questions.

I am also grateful to the entire Thin Film Group, for the pleasant working atmosphere.

Finally I want to thank my family, especially my parents for their financial and mental support through the years.

Contents

1 Theoretical aspects

1.1 Coating synthesis

1.1.1 Magnetron sputter deposition

Sputter deposition is a method of physical vapor deposition (PVD) and it is characterized by a momentum transfer process between ions from a heavy gas (typically Ar) and the surface of the target resulting in the release of material in atomic form as schematically shown in Fig. 1.1. The sputtering of the target is enabled by igniting a glow discharge between the cathode (target) and the anode which is typically the chamber wall. In order to achieve sufficiently high plasma densities in front of the target and, hence, high erosion rates, magnets are placed on the back of the target trapping the electrons in the vicinity of the target and increasing the ionization rate in this region [1]. The target of the so-called magnetron is biased to negative voltages typically between 300 to 700 V in order to provide sufficient energy to the impinging ions to sputter material from the target. The sputtered particles typically have energies ranging from 5 to 40 eV.

The substrates, on which the film will be grown, are placed in the plasma stream and sputtered atoms from the target will condense on them. To allow a gentle ion bombardment of the growing film, which is beneficial for growing dense films, an unbalanced magnetron configuration, where some of the magnetic field lines are extended to the substrate and, therefore, guiding some ions to the film growth zone, can be used. In addition, the substrates can be negatively biased with typical voltages between 20 and 100 V to enhance the ion bombardment. In order to grow nitride or oxide films, reactive gases like N_2 or O_2 can be added to the discharge. In this case, N and O atoms will react with the sputtered metal atoms on the substrate surface forming a nitride or an oxide there [1]. The industrial-scale deposition system used within this work is a magnetron sputtering device from CemeCon and is shown in Fig. 1.2.

1.1.2 Coating systems: CrAlN and CrAlSiN

Hard coatings are nowadays widely used as protective layers in industrial cutting applications to preserve the base material of the tool against oxidation and wear. They are characterized by higher hardness, higher wear resistance, better thermal stability and increased oxidation resistance in comparison to the base materials like high-speed steel or cemented carbide. The first hard coatings designed were binary nitrides and carbides such as TiC [3–6], CrN [7] and TiN [8]. The following generation were ternary nitride coatings like TiAlN and CrAlN coatings, which were developed in the 1990s to satisfy the increasing demand in higher cutting

performance [9, 10]. CrAlN-based coatings are distinguished protective coating materials for drilling tools because of their outstanding resistance against wear at elevated temperatures [11–16].

The focus of the current thesis was to study the tribological behavior of CrAlN and CrAlSiN coatings at elevated temperatures. The coatings were synthesized by direct current magnetron sputter deposition in an industrial-scale system using $Cr_{0.50}Al_{0.50}$ and $Cr_{0.45}Al_{0.45}Si_{0.10}$ composite targets (see Fig. 1.2). In the as-deposited state, CrAlN coatings typically consist of a solid solution of face-centered cubic (fcc) CrN and fcc-AlN even though these phases are immiscible in thermodynamic equilibrium and fcc-AlN would transform to the stable configuration of AlN which has a hexagonal closed packed (hcp) structure. The synthesis of metastable supersaturated phases like fcc-CrAlN by PVD methods like magnetron sputter deposition is possible due to the very high cooling rate as the atoms from the plasma condense on the substrate [1]. As shown in Fig. 1.3, the smaller Al atoms substitute the Cr atoms in the fcc lattice up to a mole fraction between 0.7-0.77. At higher Al contents, the solubility limit of AlN in fcc-CrN is exceeded and an hcp-CrAlN solid solution with the wurtzite structure of thermodynamically stable AlN is formed [17, 18].

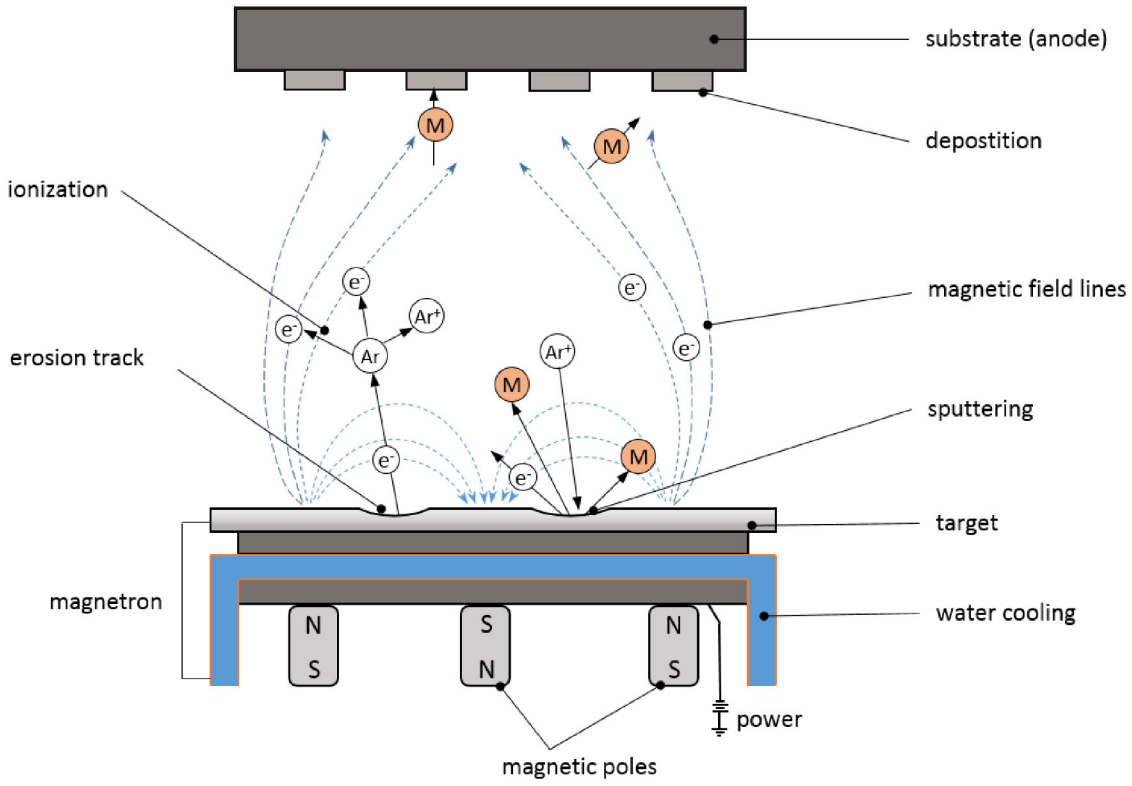

Figure 1.1: Schematic illustration of an unbalanced magnetron sputter deposition system, modified after [2].

Figure 1.2: Picture of (a) the industrial-scale magnetron sputtering CemeCon CC800/9MLT deposition plant used and (b) a powder metallurgically processed $Cr_{0.45}Al_{0.45}Si_{0.10}$ target. The carousel where the substrates were mounted is located in the center of the chamber.

Regarding the properties of CrAlN coatings, it was observed that their hardness as well as their thermal and chemical stability increased with the addition of Al. The reason for the improved mechanical properties is the solid solution hardening effect, where Al and Cr atoms are substituting each other. However this effect is limited by the above mentioned critical Al content, where the fcc crystal structure changes to the wurtzite type. Different methods and simulations, e.g., ab initio calculations or the band parameter method can be used to calculate the critical Al content [18, 20, 22].

Hardness values for fcc-CrAlN reported in literature were up to 40 GPa [23–25]. Detailed investigations of the oxidation behavior revealed the formation of a dense and adherent mixed aluminium and chromium oxide film when the CrAlN film is exposed to elevated temperatures in ambient or oxygen-containing atmospheres [11, 12, 19, 24, 26]. The onset temperature for oxidation was increased from 600 °C for CrN to 900 °C for fcc-CrAlN [11, 12, 27]. The improved mechanical properties and oxidation resistance due to the addition of Al to CrN are the main reason for the very successful application of such coatings in industrial metal cutting operations.

A further improvement of the properties of CrAlN coatings could be achieved due to the addition of Si and the formation of a nanocomposite microstructure. The concept of nanocomposite hard coatings was first successfully demonstrated for TiSiN coatings as schematically shown in Fig. 1.4. The zone model illustrates the morphology scheme of the grain size and shape as a function of the Si concentration. At very low Si contents the structure displays large elongated grains. A successive loss of preferred orientation in zone A is observed with higher Si content, which leads to the full interpenetration of both phases in zone B and isolated TiN nanocrystals in zone C [28]. In the case of CrAlSiN coatings with Si contents ranging from 10 to 20 at.%, a nanocomposite microstructure consisting of fcc-CrAl(Si)N grains, that are embedded in an amorphous SiN_x phase, is formed [28, 29]. The formation of amorphous SiN_x at the grain boundaries hinders the dislocation movement and enhances the mechanical and tribological properties of these MeN films as a result of grain size refinement according to the Hall-Petch relationship [30, 31]. With such a microstructure, values for hardness and Young's modulus of 30-40 GPa and 410-440 GPa, respectively, could be achieved [11, 12, 19, 24, 26, 32, 33].

In terms of oxidation resistance, a beneficial effect due to the formation of a SiO_x phase on the surface of the CrAlSiN coatings hindering further oxidation was noticed [23]. In this way, the onset temperature for oxidation was increased to 950 °C [27, 34]. With the mentioned improvements due to the addition of Si, the service life of CrAlSiN coated tools could be increased up to 40% compared to the ones coated with CrAlN [35].

1.2 Tribology

Tribology describes the interaction between surfaces in relative motion. It covers the scientific topics of friction, lubrication and wear which is also a characteristic field of material science. Overall, a tribological system can be seen as an energy transformation in a sliding contact.

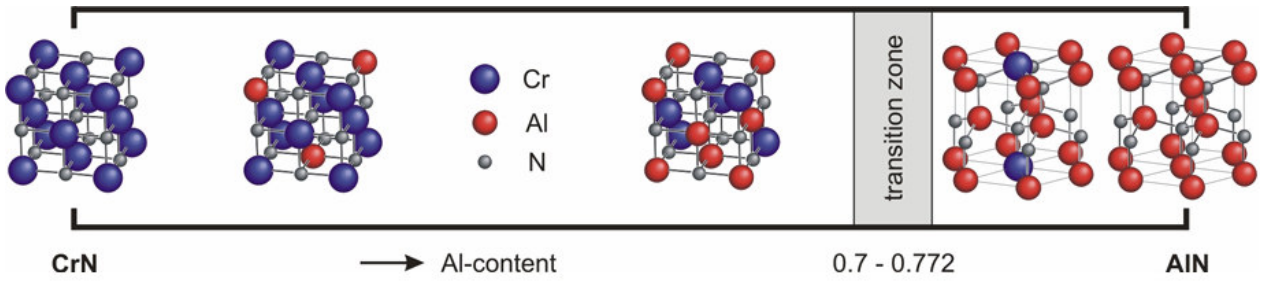

Figure 1.3: Structure evolution of CrAlN coatings deposited by PVD methods as a function of the Al content, modified after [19–21]. The transition zone from the fcc-CrAlN to hcp-CrAlN crystal structure is marked by the gray area defined by values obtained from experiments.

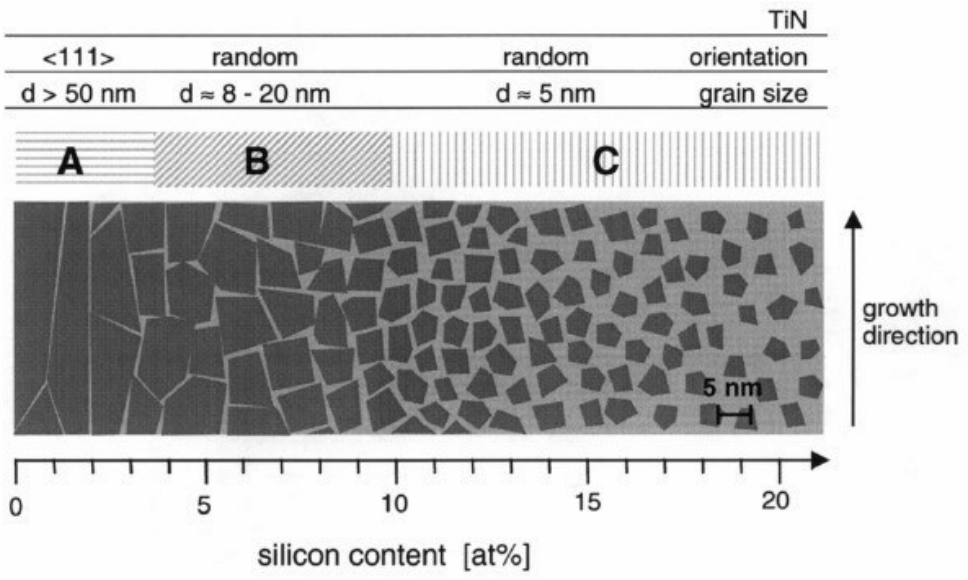

Figure 1.4: Morphological zone model for nanocystalline-TiN/amorphous-Si_3N_4 as a function of the Si content. The lighter zones represent the amorphous phase and the dark areas the nanocrystals [28].

Fig. 1.5 illustrates the tribological contact and quantification of the external input parameters converting into output parameters like friction and wear, which is also referred to as tribosystem.

Despite its importance and many centuries of research, a proper explanation for friction and wear has yet to be found. The reason for this difficulty is that the phenomenon is not a material property but a system property [36].

1.2.1 Friction

Friction is defined as the resistance to motion which a body exposes when another body in contact is moved tangentially over it. Therefore it is a system responding in the form of a reaction force which can be described with the coefficient of friction (COF). The COF is defined as the tangential frictional force F divided by the normal load w:

$$\mu = \frac{F}{w} \tag{1}$$

The frictional force F is composed of two components, namely the adhesion force between the two surfaces F_a, and the deformation force of the surfaces F_d

$$F = F_a + F_d \tag{2}$$

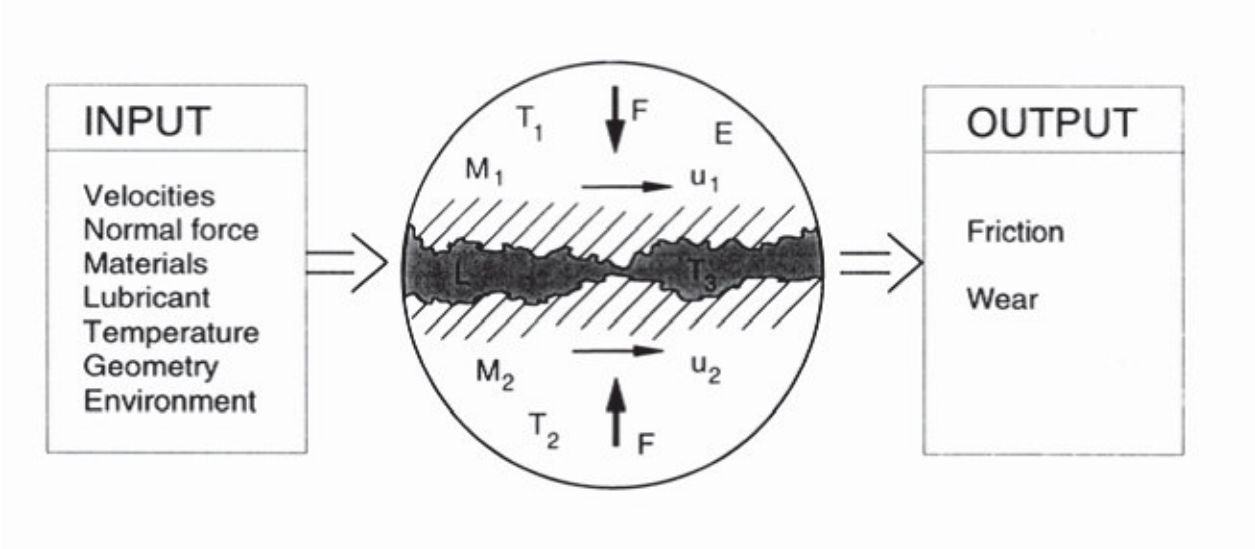

Figure 1.5: The transition of many input parameters caused by external loads in friction and wear between two bodies in relative motion [36].

Furthermore, F_d is distinguished between a "plowing friction" and an "asperity deformation", where the first term describes the macro- and the latter term the microscale [36].

Suh and Sin proposed a new concept of friction, called genesis of friction. They pointed out, that during the sliding process without a significant temperature rise, the mechanical properties show a greater impact on the friction behavior than the chemical properties. Three basic mechanisms are responsible for the effect of friction, namely asperity deformation, adhesion and plowing as shown in Fig. 1.6. The mechanism of adhesion, however, plays a minor role in many practical cases [37].

In a more explicit investigation of the microscopic mechanism of friction, Kim and Suh claimed that the most common mechanism in most sliding situations is the plowing component. This shows that the friction between two surfaces is caused by mechanical interactions at the sliding interface and by lowering the mechanical interaction, the frictional force will also be reduced. However, the microscopic models of friction are based on the view that the frictional process is a result of bond breaking of individual atoms. It is caused by strong adhesion, microasperity interlocking or slip along the weak crystal planes in the presence of crystal defects. Hence, the critical stress depends on the defects of the microscopic structure [38].

1.2.2 Types of wear

One approach to describe the wear is to classify the process by which the material is removed from the contact surface. This depends on the specific kind of movement, the geometry and the environment of the tribosystem. Examples for wear modes are rolling wear, sliding wear,

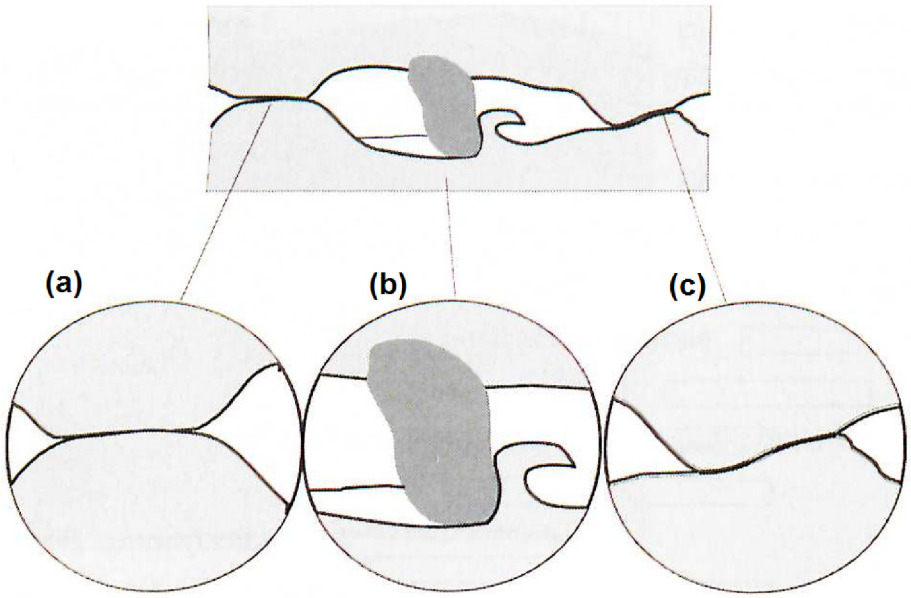

Figure 1.6: The three main effects of sliding friction are (a) adhesion, (b) plowing and (c) asperity deformation [36].

fretting, impact wear, erosion and cavitation. Since different wear modes exhibit similar, yet different influencing parameters, the similar parameters are gathered and thus varied effects can be mathematically formulated. Therefore, there is no surprise that in a real contact the wear is not only described by one single contact mechanism. There are four basic wear mechanisms as illustrated in Fig. 1.7 and described in detail in the following.

Adhesive wear When two surfaces slide over each other, the relative tangential motion causes the separation of fragments. Therefore, material from usually the softer body is removed and adheres to the counter body in the contact zone (see Fig. 1.7). These fragments may eventually fall off the surface and form loose wear particles. The "adhesive wear theory" for sliding contacts was proposed by Bowden and Tabor [39]. Early experiments were conducted on metal samples and the adhesion process was described with the term "cold welding", in which clean stripes of metals are joined together while the contact zone is deformed and stretched. Since the "welding" concept cannot be applied to nonmetals, it became preferable to use the term "adhesive wear". However, this theory cannot explain the influence of surface roughness or the creation of loose wear particles. Based on research by Suh [40], on friction and wear mechanisms, he realized that the adhesion wear mechanism does not play a dominating role in real contacts, since environmental parameters for example atmosphere, temperature and humidity have a much greater impact.

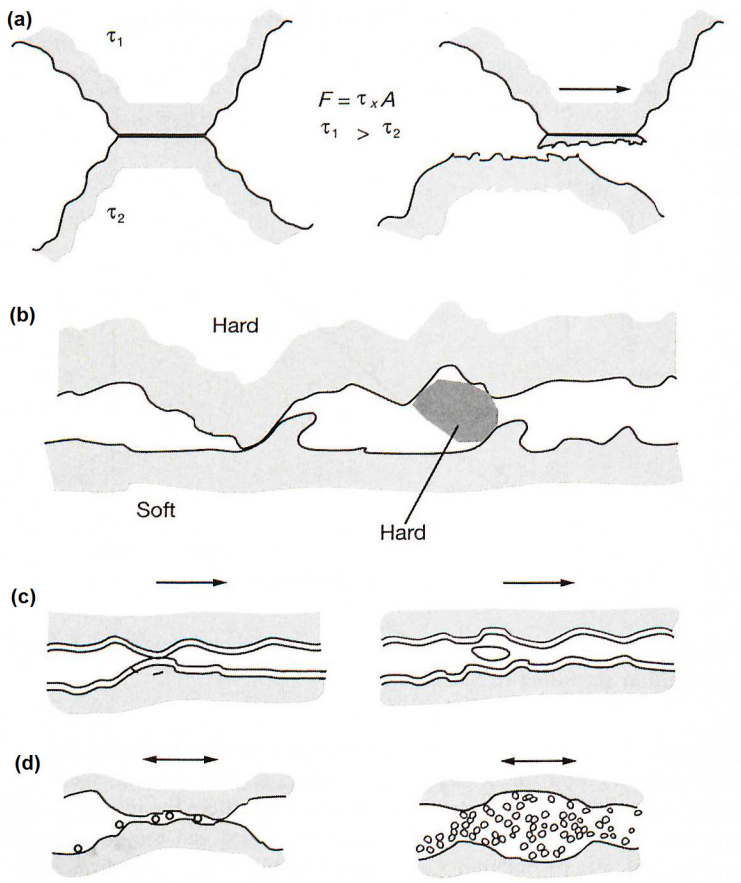

Figure 1.7: The main mechanism of wear are (a) adhesive, (b) abrasive, (c) fatigue and (d) chemical wear [36].

Abrasive wear This type of wear is distinguished between three body and two body abrasive wear, where abrasive wear caused by hard surface asperities is the reason for the latter situation. Three body abrasive wear occurs when one of the surfaces is significantly harder than the other so that the loose hard particles from the hard surface are pressed into the softer surface. The tangential movement of the two surfaces causes a plowing and removal of softer material which ultimately results in grooves or scratches in the surface. Suh [41] studied the asperity deformation mechanisms and concluded that the roughness and waviness of the opposing surfaces lead to asperity deformation. The collision of two asperities results in their plastic deformation which eventually causes material removal from the asperities.

Surface fatigue wear This type of wear can be observed after repeated rolling or sliding over a wear track. In the rolling process, the stress field is applied repeatedly over the surface and fatigue is observed in the near-surface material. Delamination on the surface, on the other hand, is caused by surface asperities repeatedly sliding over each other. The material is

exposed to a cyclic loading and unloading, which may result in the formation of subsurface or surface cracks. The first cracks may occur in the dislocated pile-ups or material voids. Once induced, these cracks may grow rapidly, unite with other cracks, break up the surface into multiple large fragments and pits and finally release surface material.

Chemical wear A wear process dominated by chemical reactions in the contact zone is called chemical wear. The most common example is the oxidational wear process. A thin layer of oxide will be formed on the freshly exposed surface when, e.g., a metal is in contact with a counter body in a humid environment. It has been found that an environment with high humidity increases the formation of the oxidation layer [42].

Kraghelsky introduced the molecular-mechanical theory of friction [43]. This theory describes the two natures of friction namely the friction of the adhesion component which includes a so-called piezo coefficient describing the increase of shear strength with compressive force. The second form of friction is the friction to overcome the material deformation component [43].

Other works have been focused more on the influence of plastic deformation of asperities. They mentioned that the resistance to motion origins from the dissipated energy for the plastic deformation of the asperities during the sliding process [44–46].

1.2.3 Tribological mechanisms in coated surfaces

A thin hard coating layer on a softer substrate has been proven to be tribologically beneficial against scratching from debris or hard particles. Therefore hard coatings act as a protective layer on the base material to improve surface properties, e.g., reduced diffusion, abrasive wear, friction and higher wear resistance. Nevertheless, the tribology of surfaces in contact and relative motion can be viewed as a process with certain input and output parameters. The origin to analyze a tribological contact lies in the input data as shown in Fig. 1.8. Characteristic input data are the geometry of the contact, the mechanical and chemical properties of the material or the environmental parameters, the relative motion, the normal load and the temperature.

During the tribological process, both physical and chemical changes to the input data occur according to the physical and chemical laws. These changes are also referred to as output parameters as illustrated in Fig. 1.8. Energy-related output effects are for example: friction, wear, temperature or changes in mechanical and surface properties. For a better understanding of the complete tribological process it is suggested to separate the changes into four different tribological effects and analyze them separately, namely macro- and microscale mechanical

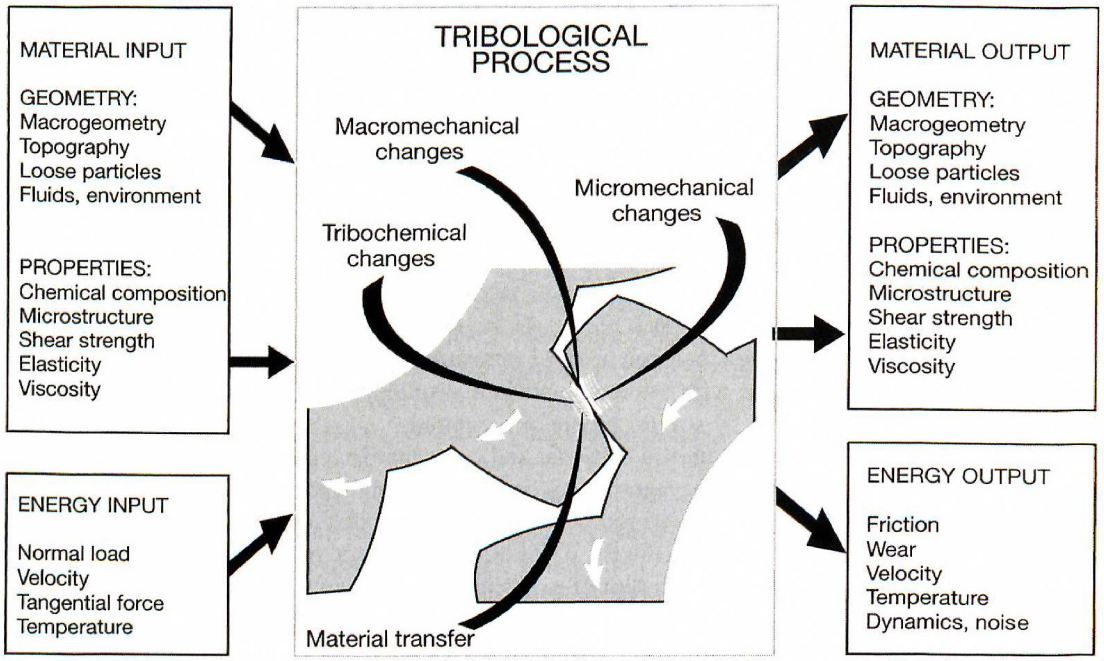

Figure 1.8: Input and output parameters during a tribological process between to surfaces [36].

effects, the chemical effects and material transfer, as shown in Fig. 1.9. Additionally, there have also been studies on the tribological behavior on a molecular level, i.e. nanophysical effects [47–49].

1.2.4 Experimental setup for tribological tests in different atmospheres

The tribological measurements of the coatings were conducted by ball-on-disc friction tests in a CSM Microtest high-temperature tribometer. The concept behind this method is to press the Al_2O_3 counterpart ball with a defined normal load of 5 N on the coated high-speed steel sample. The Al_2O_3 ball ($\varnothing$ 6 mm) was chosen due to its high wear resistance and chemical inertness even at elevated temperatures. The number of cycles was set to 6000. In order to keep the number of cycles and the angular velocity constant, the sliding distance and the linear velocity were adjusted when the radius of the wear track was changed. Prior to the test in ambient air atmosphere, the relative humidity was recorded with a hygrometer. During the tribological testing, the friction force was measured by a linear voltage displacement transducer to calculate the COF by dividing the friction force by the normal load. For each sample three tests were performed. Starting with a reference test at room temperature (RT) it was followed by the actual test at the goal temperature and closed by a comparison test at RT. The tests at elevated temperatures were performed from 100 up to 700 °C in steps

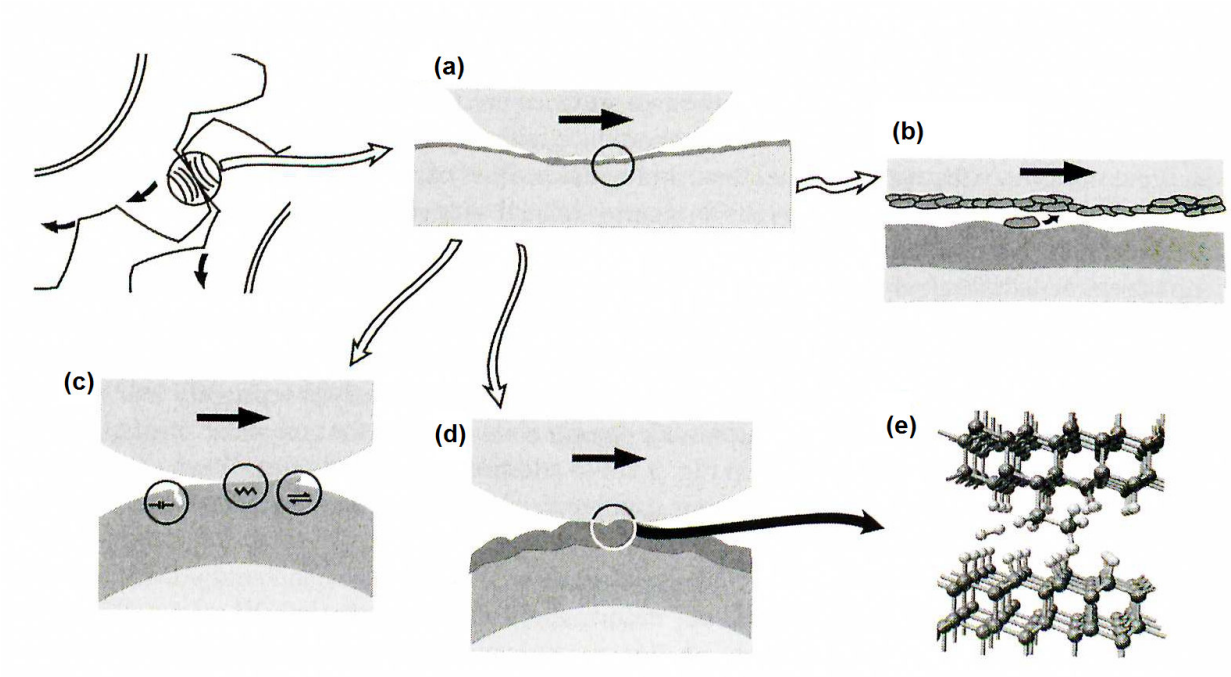

Figure 1.9: The tribological contact mechanisms are (a) macromechanical, (b) material transfer (c) micromechanical, (d) tribochemical and (e) nanophysical contact mechanisms [36].

of 100 ℃. Two sets of tests were performed, one set under ambient air atmosphere and the other set in inert atmosphere. For the testing condition in inert atmosphere the equipment was modified. To reduce the oxygen level it was necessary to isolate the sample from ambient air. For this reason a steel box with a borosilicate glass inspection panel was placed on top of the tribometer and sealed with aluminium tape for each testing set (Fig. 1.10(a)). An oxygen detector was placed inside the chamber to record the oxygen level as shown in Fig. 1.10(b). In order to establish an inert atmosphere, Ar gas from an external container was purged directly into the tribological contact zone (see schematic in Fig. 1.11) via a tube located at the bottom of the tribometer. The remaining of the sealed box was filled with N_2 introduced via a gas hose connected to the box (located at left-hand side of metal box in Fig. 1.10(a)). Prior to the test, the chamber was purged with both gases for one hour and a constant gas flow was maintained during the course of the experiment. In this way, a maximum O_2 level below 1.5 % inside the chamber could be achieved for all tests. After the test the inert gas atmosphere was maintained in order to avoid post-oxidation and to speed up the cooling process. Once the sample temperature reached a value below 70 ℃, the metal box was removed and the sample taken out for further investigations.

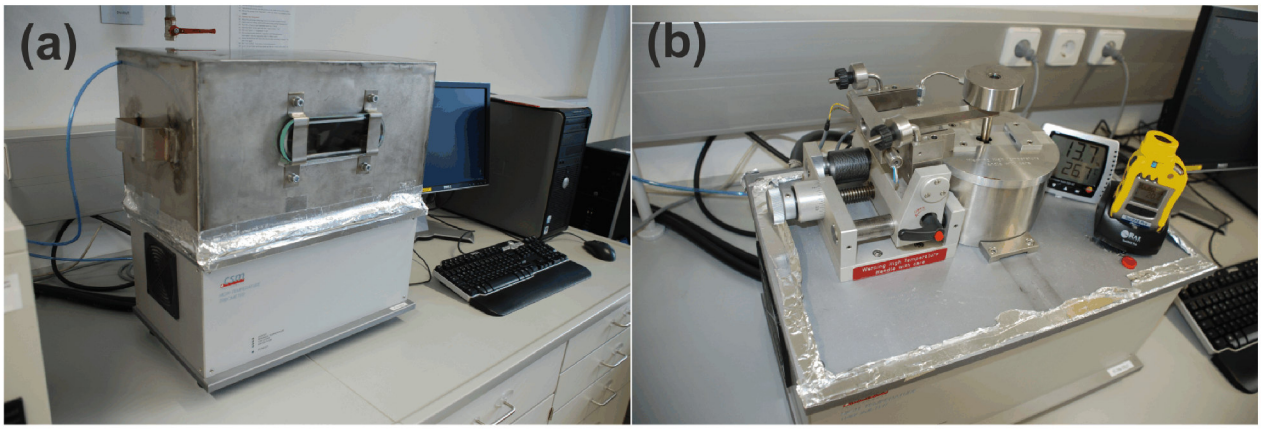

Figure 1.10: Experimental set-up showing (a) the steel box with the viewing panel and the N_2 tube and (b) the sample chamber with the hygrometer and oxygen detector.

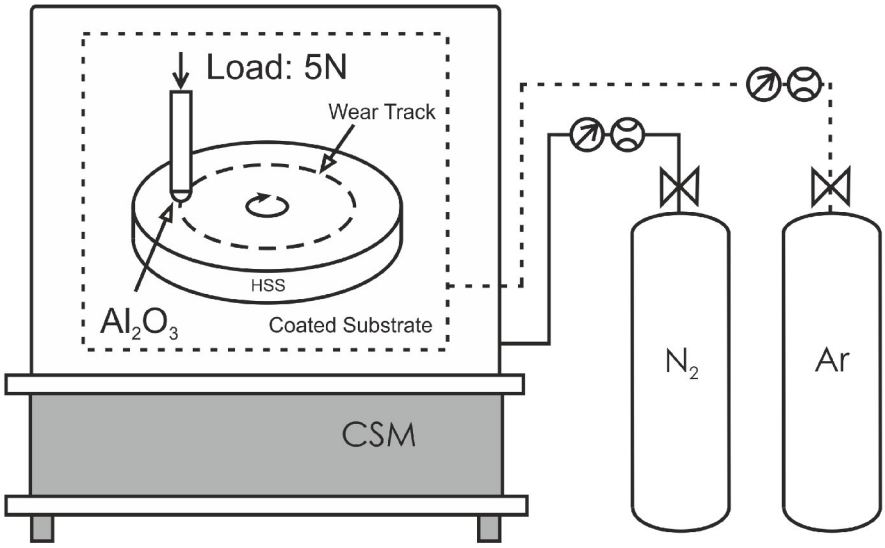

Figure 1.11: Scheme of the experimental setup used for the tribological test at elevated temperatures in inert atmosphere. Ar gas (dashed line) flows directly into the tribological contact zone, whereas the N_2 (solid line) purges the whole box.

1.3 Raman spectroscopy

Raman spectroscopy is an analysis technique that can provide chemical information without damaging the sample. Typically, the sample of interest is illuminated with laser light. The majority of the light (99,9%) is transmitted through the sample or absorbed. Only a small part is scattered elastically by molecules or crystal lattices at the same wavelength which is referred to as Rayleigh scattering. Spectral analysis shows an intense spectral line matching the wavelength of the light source. The weak Raman scattering (inelastically scattered light) interacts with the atomic electron shell which is a signature of the sample. Compared to

Rayleigh scattering and fluorescence, the Raman scattering intensities are several orders of magnitudes lower [50, 51]. The observed weaker peaks are shifted, compared to the wavelength of the light source due to the interaction of the incident light with phonons in the analyzed material. The bands shifted to higher wave numbers (typically given in cm^{-1}) are called Anti-Stokes Raman bands and bands shifted to lower wave numbers are called Stokes Raman bands. Usually the intensities of the Stokes shifted Raman bands are more intense and are therefore used for qualitative and/or quantitative analysis. Within this work, Raman spectroscopy was used to investigate the oxidation products which were formed in the tribological contact zone when testing the CrAlN and CrAlSiN coatings.

References

[1] M. Ohring, Materials Science of Thin Films, 2nd Edition, Academic Press, San Diego, USA, 2001.

[2] W. D. Sproul, Surface and Coatings Technology 49 (1-3) (1991) 284–289.

[3] J.-E. Sundgren, Thin Solid Films 128 (1-2) (1985) 21–44.

[4] S. Wilson, A. Alpas, Surface and Coatings Technology 108-109 (1998) 369–376.

[5] S. Wilson, A. Alpas, Surface and Coatings Technology 120-121 (1999) 519–527.

[6] S. Wilson, A. Alpas, Wear 245 (1-2) (2000) 223–229.

[7] B. Navinšek, P. Panjan, I. Milošev, Surface and Coatings Technology 97 (1-3) (1997) 182–191.

[8] Z. Zhou, W. Rainforth, Q. Luo, P. Hovsepian, J. Ojeda, M. Romero-Gonzalez, Acta Materialia 58 (8) (2010) 2912–2925.

[9] W. Münz, S. Reineck, K. Harting, in: Proceedings of the 7th International Conference on Vacuum Metallurgy, Tokyo, Japan, 1982, pp. 633–640.

[10] O. Knotek, M. Böhmer, T. Leyendecker, Journal of Vacuum Science and Technology A 4 (6) (1986) 2695.

[11] A. Reiter, V. Derflinger, B. Hanselmann, T. Bachmann, B. Sartory, Surface and Coatings Technology 200 (7) (2005) 2114–2122.

[12] H. C. Barshilia, N. Selvakumar, B. Deepthi, K. Rajam, Surface and Coatings Technology 201 (6) (2006) 2193–2201.

[13] M. Brizuela, A. Garcia-Luis, I. Braceras, J. I. Oñate, J. C. Sánchez-López, D. Martínez-Martínez, C. López-Cartes, A. Fernández, Surface and Coatings Technology 200 (1-4 SPEC. ISS.) (2005) 192–197.

[14] O. Banakh, P. Schmid, R. Sanjinés, Surface and Coatings Technology 163-164 (2003) 57–61.

[15] J. C. Sanchez-Lopez, D. Martinez-Martinez, C. Lopez-Cartes, A. Fernandez, M. Brizuela, A. Garcia-Luis, J. I. Onate, Journal of Vacuum Science and Technology A 23 (4) (2005) 681.

[16] J. Lin, B. Mishra, J. J. Moore, W. D. Sproul, Surface and Coatings Technology 201 (7) (2006) 4329–4334.

[17] A. Kimura, M. Kawate, H. Hasegawa, T. Suzuki, Surface and Coatings Technology 169-170 (2003) 367–370.

[18] A. Sugishima, H. Kajioka, Y. Makino, Surface and Coatings Technology 97 (1997) 590–594.

[19] A. E. Reiter, C. Mitterer, B. Sartory, Journal of Vacuum Science and Technology A 25 (4) (2007) 711.

[20] Y. Makino, K. Nogi, Surface and Coatings Technology 98 (1-3) (1998) 1008–1012.

[21] M. Hirai, T. Suzuki, H. Suematsu, W. Jiang, K. Yatsui, Journal of Vacuum Science and Technology A 21 (4) (2003) 947.

[22] P. Mayrhofer, D. Music, T. Reeswinkel, H.-G. Fuß, J. Schneider, Acta Materialia 56 (11) (2008) 2469–2475.

[23] C. Tritremmel, R. Daniel, M. Lechthaler, P. Polcik, C. Mitterer, Thin Solid Films 534 (2013) 403–409.

[24] H. Willmann, Al-Cr-N thin film design for high temperature applications, Ph.D. thesis, Montanuniversität Leoben (2007).

[25] J. C. Sánchez-López, A. Contreras, S. Domínguez-Meister, A. García-Luis, M. Brizuela, Thin Solid Films 550 (2014) 413–420.

[26] A. E. Reiter, C. Mitterer, M. Rebelo de Figueiredo, R. Franz, Tribology Letters 37 (3) (2010) 605–611.

[27] T. Polcar, A. Cavaleiro, Materials Chemistry and Physics 129 (2011) 195–201.

[28] J. Patscheider, T. Zehnder, M. Diserens, Surface and Coatings Technology 146 (2001) 201–208.

[29] J. L. Endrino, S. Palacín, M. H. Aguirre, A. Gutiérrez, F. Schaefers, Acta Materialia 55 (6) (2007) 2129–2135.

[30] J. Musil, Surface and Coatings Technology 125 (1-3) (2000) 322–330.

[31] E. Arzt, Acta Materialia 46 (16) (1998) 5611–5626.

[32] S. Zhang, L. Wang, Q. Wang, M. Li, Surface and Coatings Technology 214 (2013) 160–167.

[33] Z. Yuan, L. Sun, Q. Fang, W. Gong, X. Wu, Z. Xu, Thin Solid Films 594 (2015) 18–23.

[34] Y.-Y. Chang, C.-Y. Hsiao, Surface and Coatings Technology 204 (6-7) (2009) 992–996.

[35] W. Wu, W. Chen, S. Yang, Y. Lin, S. Zhang, T.-Y. Cho, G. Lee, S.-C. Kwon, Applied Surface Science 351 (2015) 803–810.

[36] K. Holmberg, A. Matthews, Coatings Tribology: Properties, Mechanisms, Techniques and Applications in Surface Engineering, Elsevier, Amsterdam, Netherlands, 2009.

[37] N. P. Suh, H.-C. Sin, Wear 69 (1) (1981) 91–114.

[38] D. Kim, N. Suh, Wear 149 (1-2) (1991) 199–208.

[39] F. P. Bowden, D. Tabor, The Friction and Lubrication of Solids, Clarendon Press, Oxford, UK, 1986.

[40] N. P. Suh, Wear 25 (1) (1973) 111–124.

[41] N. Suh, Tribophysics, Prentice Hall, Englewood Cliffs, New Jersey, 1986.

[42] E. Rabinowicz, Friction and Wear of Materials, John Wiley and Sons, New York, 1965.

[43] I. V. Kraghelsky, Wear 9 (5) (1966) 408.

[44] D. Rigney, J. Hirth, Wear 53 (2) (1979) 345–370.

[45] P. Heilmann, D. Rigney, Wear 72 (2) (1981) 195–217.

[46] A. Green, Proceedings of the Royal Society A 228 (1173) (1955) 191–204.

[47] S. Hsu, Z. Ying, Nanotribology: Critical Assessment and Research Needs, Springer Science and Business Media, New York, USA, 2012.

[48] B. Bhushan, Fundamentals of tribology and bridging the gap between the macro- and micro/nanoscales, Springer Netherlands, Dordrecht, Netherlands, 2012.

[49] B. Bhushan, J. N. Israelachvili, U. Landman, Nature 374 (6523) (1995) 607–616.

[50] E. Smith, G. Dent, Modern Raman Spectroscopy A Practical Approach, Wiley and Sons Ltd, Chichester, United Kingdom, 2005.

[51] I. DeWolf, Semiconductor Science and Technology 11 (2) (1996) 139–154.

2 Manuscript

2.1 Introduction

CrAlN-based hard coatings have been established as protective layers in industrial cutting applications to preserve the base material of the tool against oxidation and wear. By alloying the binary CrN with Al, enhanced mechanical properties can be achieved as a result of solid solution hardening, as long as the face-centered cubic (fcc) structure of CrN is maintained [1, 2]. The solubility of AlN in fcc-CrN is typically restricted to 70-77 at.%, while at higher AlN contents, the hexagonal wurtzite type structure of AlN appears [3, 4].

CrAlN is more oxidation resistant than CrN due to a dense, protective oxide layer that forms on the coating surface during annealing in oxygen containing atmosphere [2, 5]. With the addition of Si, a nanocomposite of crystalline CrAl(Si)N grains and an amorphous SiN_x grain boundary phase can be formed resulting in further improvement of the mechanical properties [6]. The formation of a SiO_x phase during oxidation further enhances the protective effects of the thin oxide layer on the surface of the coating [7]. Because of these outstanding properties, CrAlN and CrAlSiN coatings are designated for the use in industrial cutting applications [2, 8, 9].

The tribological properties of these coatings at high temperature have already been studied to some extent in previous works. Polcar et al. investigated the tribological behavior of CrAlN and CrAlSiN coatings from room temperature (RT) up to 500 ℃ using Al_2O_3 balls as counterparts [10, 11]. The average friction for the CrAlN coating was higher in the temperature range between 100 and 400 ℃, but decreased at higher temperatures. On the other hand, the wear rate of the coating moderately increased with increasing temperature. Compared to CrAlN, the coefficent of friction (COF) for CrAlSiN coatings were higher above 300 ℃, but the friction curves were smoother. The obtained wear rates of the coatings were generally lower, but the film was worn through at lower temperatures due to adhesive film failure. However, the above mentioned experiments were all performed in ambient air atmosphere. Although CrAlN and CrAlSiN coatings are oxidation resistant at elevated temperature, surface oxidation for both CrAlN and CrAlSiN coatings might already occur in the tribological contact zone due to significantly higher flash temperatures if the protective oxide layer on the surface is worn off and the fresh coating material is exposed [12].

The goal of the present work was to analyze the tribological behavior of CrAlN and CrAlSiN coatings in ambient and inert atmosphere at elevated temperatures. The reason for the two different atmospheres was to study the types of wear mechanisms, i.e. abrasive and oxidation wear. In ambient atmosphere a combination of abrasive and oxidative wear can be expected, whereas wear in inert atmosphere is mainly abrasive. Raman analysis of the wear

scars on the wear and counterparts revealed further information about the wear mechanisms.

2.2 Experimental details

The CrAlN and CrAlSiN coatings were deposited in an industrial-scale deposition plant CemeCon CC800/9MLT using bipolar pulsed direct current magnetron sputtering. Four targets with compositions of either $Cr_{0.50}Al_{0.50}$ or $Cr_{0.45}Al_{0.45}Si_{0.10}$ were used in each deposition run with a constant power of 6 kW. The total deposition pressure in the chamber was set to 0.62 Pa and the gas flow rate was adjusted to 230 sccm for Ar and 146 sccm for N_2. The substrate holder with the high-speed steel (HSS, DIN 1.3343, AISI M2) and Silicon (Si) substrates was negatively biased with a voltage of 60 V and the substrate temperature was regulated to 540 ℃. Prior to deposition, the HSS coupons (30 mm × 10 mm) were ground and polished up to 1 µm finish and ultrasonically cleaned in an acetone and ethanol bath. In addition, the substrates were plasma etched in a pure Ar plasma. The deposition time was set to 110 min for the $Cr_{0.50}Al_{0.50}$ and 130 min for the $Cr_{0.45}Al_{0.45}Si_{0.10}$ targets.

The adhesion of the coatings was evaluated via the Rockwell C indents method according to VDI 3198 [13, 14] using a Mitutoyo DT-10 hardness tester and the thickness of the coating was measured by the ball crater method. Subsequently, the morphology of the coatings was assessed in a Zeiss Evo 50 scanning electron microscope (SEM) by recording fracture cross-section and surface images. The composition of the coatings was determined by energy dispersive X-ray spectroscopy (EDX) using the Oxford Instruments INCA EDX system attached to the SEM. The coating structure was characterized via X-ray diffraction (XRD) using a Bruker D8 Advance diffractometer in parallel beam geometry with a grazing incidence of 5°. The device was equipped with a Cu-K ceramic tube (wavelength: 0.154056 nm) and an energy-dispersive detector (SolX from Bruker AXS).

The mechanical properties of the thin films were evaluated by nanoindentation using an Ultra Micro Indentation System (UMIS, Fischer-Cripps Laboratories) with a Berkovich indenter and applying a maximum load of 30 mN. From the recorded load-displacement curves, hardness and Young's modulus of the films were calculated according to the Oliver and Pharr method [15]. The tribological properties of the coatings were investigated in ambient air atmosphere as well as in Ar + N_2 inert atmosphere in a CSM Microtest high-temperature tribometer at room temperature (RT) and at high temperature (HT) starting from 100 up to 700 ℃ in steps of 100 ℃. Before each test, the relative humidity as recorded with a Testo 608 H1-Hygrometer was in the range from 30 to 40% for the tests in ambient atmosphere. For the inert atmosphere the relative humidity was reduced to 0% and the O_2 level was measured with a ToxiRAE Pro oxygen detector. The tests performed in a controlled inert atmosphere had an additional steel box which was sealed with aluminium tape during the experiment. In this

sealed box, the tribological contact zone was floated with Ar and the rest of the chamber was purged with N_2 for approximately 1 h prior to testing, allowing the O_2 level in the chamber to drop below 1.5% to prevent oxidation of the coating during HT tribological testing. The mixture of Ar and N_2 gas was used to optimize the purging time since N_2 supply offered higher flow rates than the Ar supply. For each sample 3 tests were performed. A reference test was performed at RT followed by the actual test at the goal temperature and ended with a comparison test at RT. The number of laps was set to 6000 and a normal load of 5 N was applied. In order to keep the number of laps and the angular velocity constant, the sliding distance and the linear velocity were adjusted when the wear track radius was changed as shown in Table 2.1.

Table 2.1: Parameters used in the tribological tests of CrAlN and CrAlSiN in ambient air and inert atmosphere for the temperature sequence RT-HT-RT.

	radius [mm]	linear velocity [cm·s^{-1}]	sliding distance [m]
RT	3	4.3	113
HT	5	7.14	189
RT	7	10	264

Sintered polycrystalline Al_2O_3 balls (purity of 99.8% and ⌀ 6 mm) were chosen as counter bodies due to their chemical inertness within the temperature range of interest. During the tribological testing, the friction force was measured by a linear voltage displacement transducer and the coefficient of friction (COF) calculated by dividing the friction force by the normal load.

Afterwards, the wear volume of the coatings was evaluated by an optical 3D white light profiling system (Wyko NT 1000) and the wear coefficients were calculated as the ratio between the wear volume and the applied load times the sliding distance [12, 16]. Images of the coatings' wear tracks and the wear scars on the counterparts were taken using light optical microscopy. A HORIBA Jobin Yvon LabRam-HR800 Raman spectrometer equipped with a frequency-doubled Nd-YAG laser (532.07 nm, 100 mW) was used to identify qualitative information of materials formed in the contact zone during tribological testing. The reference peak position were taken from [17–21].

Table 2.2: The chemical composition of CrAlN and CrAlSiN obtained by EDX.

	Cr [at.%]	Al [at.%]	Si [at.%]	N [at.%]
CrAlN	23.9	25.1	-	51.0
CrAlSiN	21.6	22.1	4.5	51.8

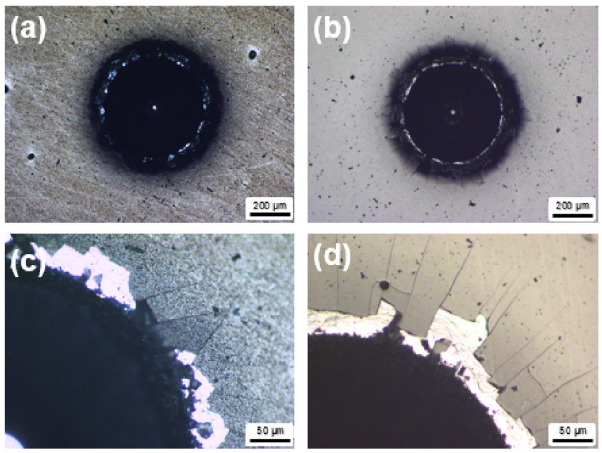

Figure 2.1: Light optical microscope images of the Rockwell C indents on CrAlN (a)+(c) and CrAlSiN (b)+(d) coatings deposited on HSS.

2.3 Results and discussion

2.3.1 Coating characterization

The adhesion of the coatings were classified from the images of the Rockwell C indents in Fig. 2.1 as HF 2 for the CrAlN and HF 3-4 for the CrAlSiN coating. The film thicknesses were 4.4 µm for CrAlN and 5.5 µm for CrAlSiN. The reason for the different thicknesses lies in the slightly varying deposition rates of 40 nm/min for CrAlN and 42 nm/min for CrAlSiN, but mainly in the longer deposition time for the CrAlSiN coating.

Since the target composition is typically reflected in the composition of sputter deposited coatings, a similar chemical composition of the coatings was obtained, as given in Table 2.2. It should be mentioned that for both coating systems the nitrogen content was about 50 at.% which indicates that the coatings are stoichiometric.

The XRD patterns recorded for the deposited CrAlN and CrAlSiN coatings are shown in Fig. 2.2. Both films exhibit a fcc crystal structure with the diffraction peaks located between fcc-AlN and fcc-CrN but with a high tendency towards fcc-CrN. The diffractogram for CrAlN shows two dominating peaks, i.e. (111) and (200), and several less intense peaks, whereas the CrAlSiN diffractogram shows a distinctive smaller (200) fcc-CrN peak.

Subsequently, the morphology was assessed by SEM as shown in Fig. 2.3 (a) and (b).

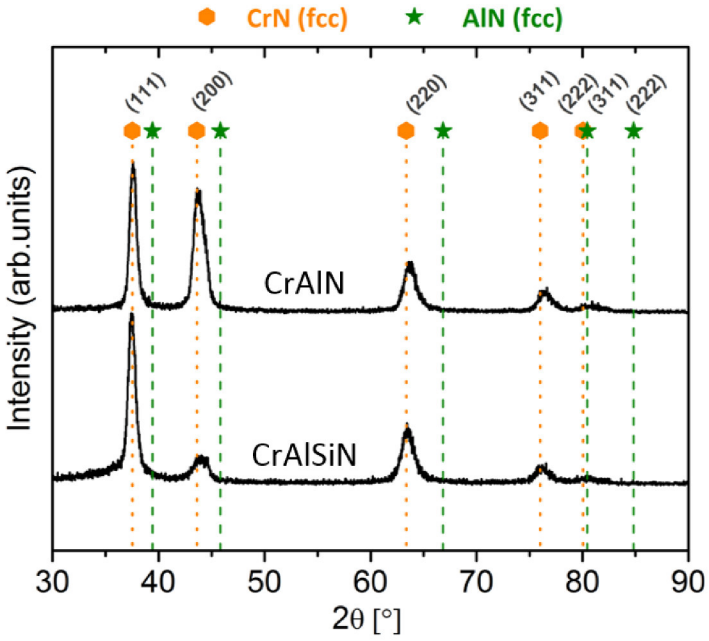

Figure 2.2: XRD diffractograms of the as-deposited CrAlN and CrAlSiN coatings. Reference peak positions are given according to the International Centre for Diffracton Data (ICDD) for the materials CrN (ICDD card no. 03-065-2899) and AlN (ICDD card no. 03-065-0841).

Table 2.3: Hardness H and Young's modulus E_s of CrAlN and CrAlSiN on HSS.

	H [GPa]	E_s [GPa]
CrAlN	22.7 ± 1.8	409 ± 32
CrAlSiN	34.3 ± 1.6	441 ± 14

The SEM top-view images revealed a rougher surface for CrAlN in comparison to the rather smooth CrAlSiN surface. The reason for this behavior is the columnar growth in the CrAlN coating as can be observed in Fig. 2.3 (c). This growth mode is interrupted by the addition of Si to the CrAlN lattice in the CrAlSiN coating [7] resulting in a smoother coating surface.

Table 2.3 shows the hardness and Young's modulus measured by nanoindentation. The higher values of CrAlSiN compared to CrAlN are a result of the nanocomposite structure consisting of fcc-CrAl(Si)N crystallites in an amorphous SiN_x matrix resulting in a hardening of the film [2, 7, 22].

2.3.2 Tribological properties

The tribological tests for both coatings were first performed in ambient air atmosphere as shown in Fig. 2.4. Starting with the tests at RT, it was observed that during the running-in

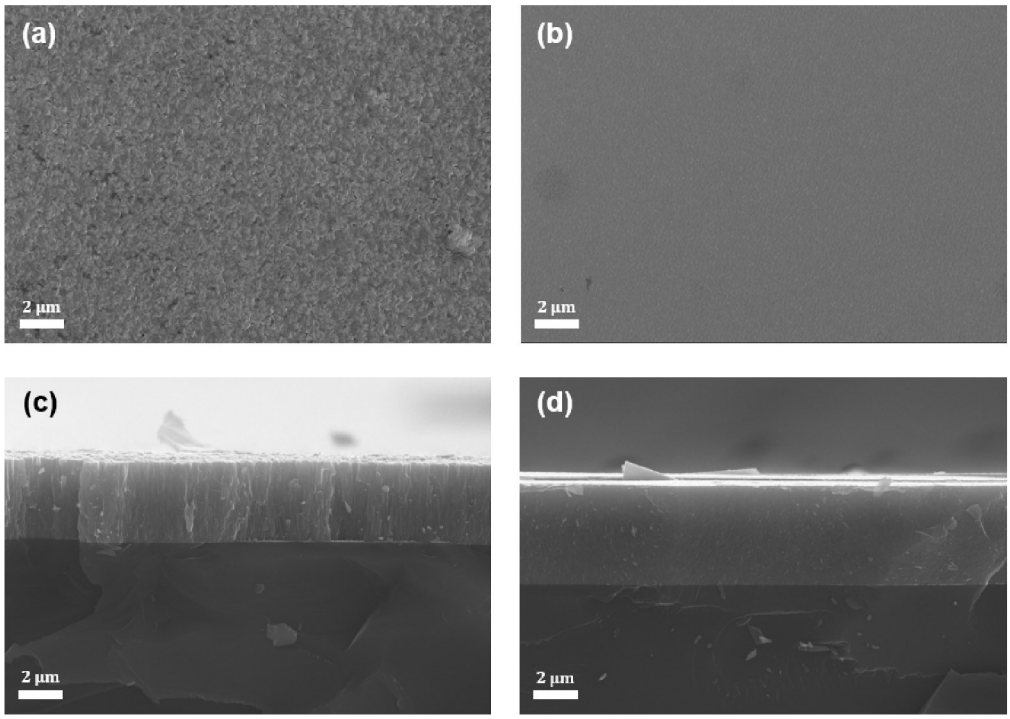

Figure 2.3: SEM top-view images of (a) CrAlN and (b) CrAlSiN as well as fracture cross-section images of (c) CrAlN and (d) CrAlSiN deposited on Si.

period, which lasted for approximately 100 laps, a rapid increase of the COF for the CrAlN coating was noticed, followed by a steady-state period, where the COF remained unaltered for the rest of the test. The COF of the CrAlN coating in ambient air atmosphere reached values of around 0.5 at RT and generally increased with increasing temperature up to 700 ℃. The maximum value of ~ 0.8 was measured at 100 and 600 ℃. At 700 ℃, the highest testing temperature, the COF was recorded with the value of ~ 0.6. Above 300 ℃ a strong scattering of the COF has been noticed during the tests. This fluctuation most likely originates from the accumulation of wear debris in front of the contact zone between counterpart and coating as it was noticed before in similar experiments [23–26]. The corresponding depths of the wear tracks were low (see 3D wear track profiles in Fig. 2.4), from RT up to 600 ℃ they were below 1 µm. The measured wear track depth at 700 ℃ showed a pronounced wear track which indicates that the coating was partially removed from the sample.

The evolution of the COF for the CrAlN coating in inert atmosphere was similar to the one in ambient air atmosphere (see Fig. 2.4). With increasing temperature from RT to 300 ℃ the COF rose up to a value of ~ 0.9. In addition to the high friction, a pronounced scattering of the COF was noticed at 300 ℃. The scattering remained unaltered for further increasing of the temperature up to 600 ℃, but the values of the COF slightly decreased to ~ 0.7. At the maximum temperature of 700 ℃, the COF was ~ 0.6 with reduced scattering. The wear

tracks on the CrAlN coating from RT to 200 ℃ were hardly noticeable. At 300 ℃ a shallow wear track was present, but at 400 ℃ a wear depth in the range of the coating thickness was observed. At even higher temperatures, from 500 to 700 ℃, the measured wear tracks became slightly wider but the wear depth decreased.

When tested in ambient air atmosphere, the CrAlSiN coating exhibited a comparable behavior as CrAlN (see Fig. 2.5). From RT to 300 ℃ the COF was generally low. However, at 400 ℃ the COF scattered strongly between 0.8 and 1.2 during the first stage of the steady-state period and eventually settled at 1.2. From 500 to 600 ℃ the COF remained high with values between 0.9 and 1, but, similar to CrAlN, it decreased to about 0.5 at 700 ℃. According to the wear track profiles in Fig. 2.5, hardly any noticeable wear was recorded from RT to 500 ℃, whereas at 600 and 700 ℃ a great part of the coating was removed during the test. In the case of the test at 600 ℃, the shape of the wear track and the fact that the deep groove was non-continuous along the wear track indicate that mainly adhesion problems caused the observed strong wear. Contrarily, at 700 ℃ the wear was due to common wear mechanisms like, e.g., abrasion or oxidation.

The recorded COF for the CrAlSiN coating in inert atmosphere showed a comparable rising COF between RT and 300 ℃ smilar to the tests in ambient air. At 300 ℃ the COF reached a maximum value of ~ 0.9 but showed pronounced scattering at two time intervals during the test. With further increasing the temperature, the scattering of the COF became even more pronounced, but the values for the COF decreased. In terms of wear, no apparent wear track could be noticed from RT to 300 ℃ and at 500 ℃ only a very shallow wear track could be measured. In contrast, deep grooves were present on the CrAlSiN coatings after testing at 400 and 600 ℃. However, their shape with steep flanks and depths comparable to the coating thickness also indicate adhesion problems as it was the case for the test in ambient air atmosphere at 600 ℃. The wear track after testing at 700 ℃ in inert atmosphere was broad, but with a homogeneous depth along the wear track cross-section.

Since the COF showed partially different trends at elevated temperature, it was of great interest to figure out, if the coating was affected by the testing at higher temperature. Therefore, RT tests on each coating were performed prior and after testing at HT as shown in Figs. 2.6 and 2.7. The variation of the COF values of CrAlN before testing at HT was minimal in both testing atmospheres. After annealing to HT, the situation remained unchanged in the case of the tests in inert atmosphere. After testing in ambient air the COFs slighty increased in general, but mainly the variation of the COF values increased. Apparently, the CrAlN coating were more affected due to the tests in ambient air than in inert atmosphere, but the change in friction behavior due to annealing was only slight in all cases.

A similar friction behavior was observed for the CrAlSiN samples (see Fig. 2.7). In terms

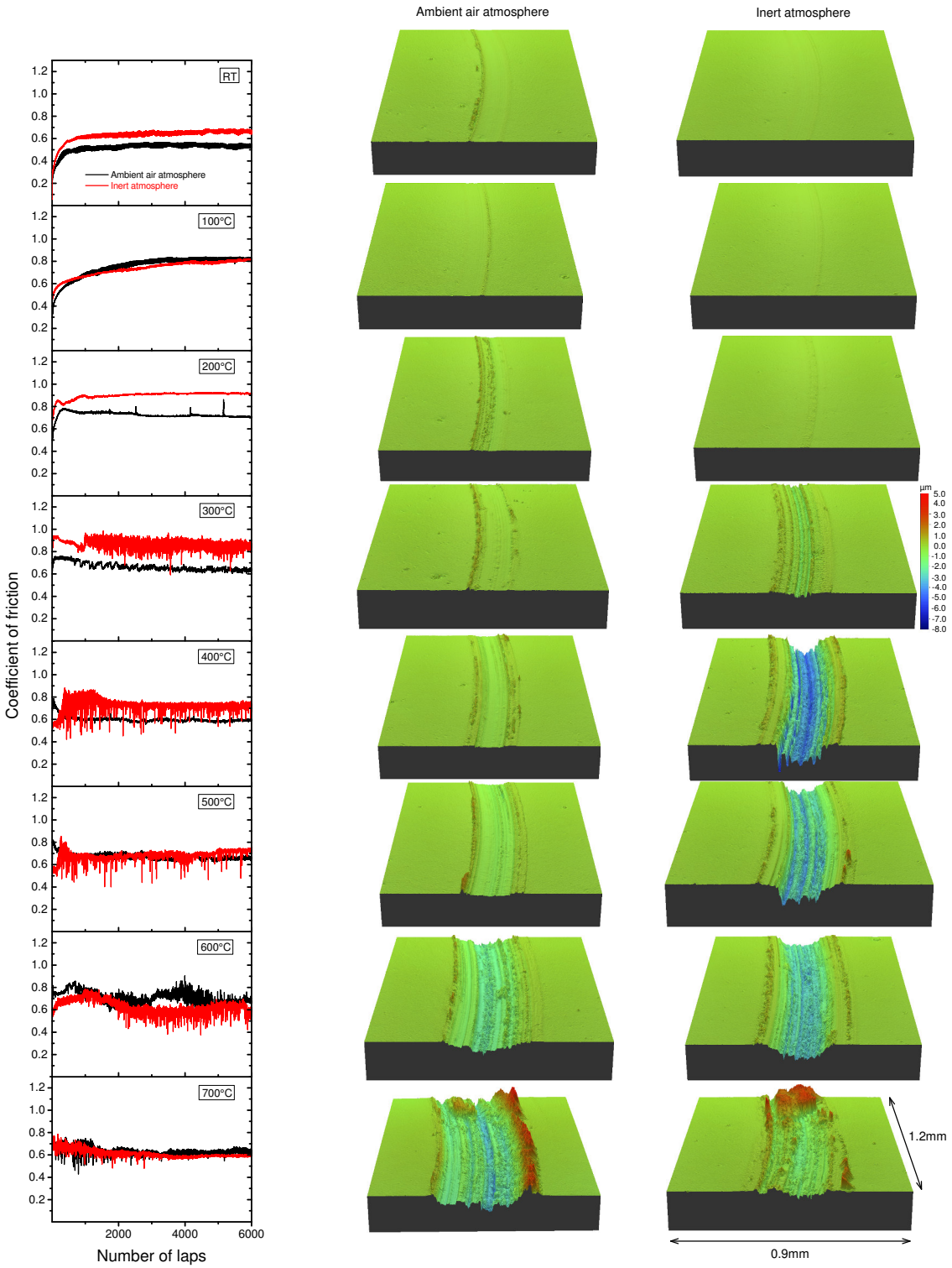

Figure 2.4: COF vs. number of laps measured on CrAlN coatings from RT to 700 ℃ in ambient air and inert atmosphere (left column). 3D profiles of the wear tracks on the coating after testing in ambient air (central column) and inert atmosphere (right column).

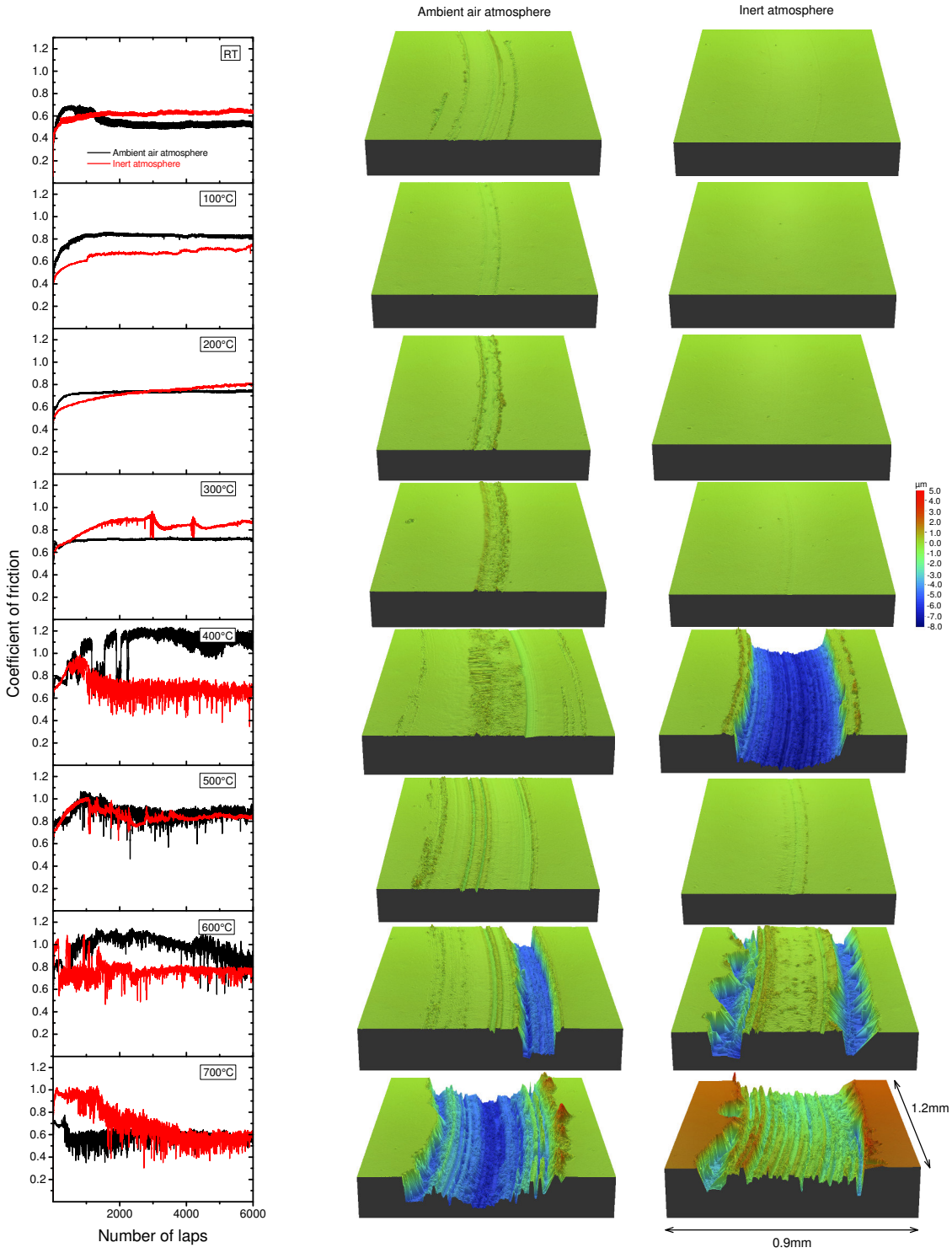

Figure 2.5: COF vs. number of laps measured on CrAlSiN coatings from RT to 700 ℃ in ambient air and inert atmosphere (left column). 3D profiles of the wear tracks on the coating after testing in ambient air (central column) and inert atmosphere (right column).

of wear, no apparent wear track could be noticed from RT to 300 ℃ and at 500 ℃ only a very shallow wear track could be measured. In contrast, deep grooves were present on the CrAlSiN coatings after testing at 400 and 600 ℃. However, their shape with steep flanks and depths comparable to the coating thickness also indicates adhesion problems as it was the case for the test in ambient air at 600 ℃. The wear track after testing at 700 ℃ in inert atmosphere was broad, but with a homogeneous depth along the wear track cross-section. The variation of the COF values prior to annealing was greater than in the case of CrAlN and after annealing the COFs in ambient air atmosphere were slightly higher, whereas in inert atmosphere the friction was slightly reduced. However, also the CrAlSiN coatings were more affected due to annealing in ambient than in inert conditions.

In order to evaluate the wear resistance, the wear coefficients from all coatings wear tracks and counterparts were calculated. Starting with the CrAlN coating in ambient air atmosphere, as shown in Fig. 2.8(a), all coating wear coefficients remained below $1{\cdot}10^{-17}m^3{\cdot}N^{-1}{\cdot}Lap^{-1}$ from RT to 300 ℃. Raising the temperature up to 700 ℃, the wear increased by two orders of magnitude and, hence, the highest wear was observed at the maximum testing temperature of 700 ℃. The obtained wear coefficients of the Al_2O_3 counterparts are presented in Fig. 2.8(b), which were one order of magnitude lower than the corresponding wear coefficients of the coatings, but also increased in general with increasing temperature. Only at 300 and at 500 ℃ the ball wear was strongly reduced without apparent correlation to the coating material or the test conditions.

The wear coefficients of the CrAlN coating in inert atmosphere were also low at the temperatures ranging from RT to 200 ℃. However, at 300 ℃ the wear increased by one order of magnitude and continuously increased until it reached a plateau at about $7{\cdot}10^{-16}m^3{\cdot}N^{-1}{\cdot}Lap^{-1}$ between 400 and 600 ℃. At 700 ℃ the coating wear reduced to a value of $1{\cdot}10^{-16}m^3{\cdot}N^{-1}{\cdot}Lap^{-1}$. The corresponding wear coefficients of the balls slightly rose with increasing temperature but remained at about $1{\cdot}10^{-17}m^3{\cdot}N^{-1}{\cdot}Lap^{-1}$ up to 700 ℃.

CrAlSiN displayed a very low wear coefficient in ambient air, starting from RT to 500 ℃ (see Fig. 2.9(a)). At 600 ℃ the wear coefficient started to increase and reached its maximum of $2{\cdot}10^{-15}m^3{\cdot}N^{-1}{\cdot}Lap^{-1}$ at 700 ℃. It has been noticed that only at 600 ℃ a strong scattering of the wear coefficient occurred which is due to an uneven material removal along the wear track caused by the adhesion problems. The wear coefficient of the Al_2O_3 balls was low up to 300 ℃, but strongly increased to $5{\cdot}10^{-15}m^3{\cdot}N^{-1}{\cdot}Lap^{-1}$ at 400 ℃ and remained high at temperatures above.

In inert atmosphere the wear coefficients of the CrAlSiN coatings nearly showed the exact same trend from RT to 700 ℃ as it was the case in ambient air atmosphere, but the absolute values were generally lower. The only noticeable exception were at 400 and 600 ℃ where

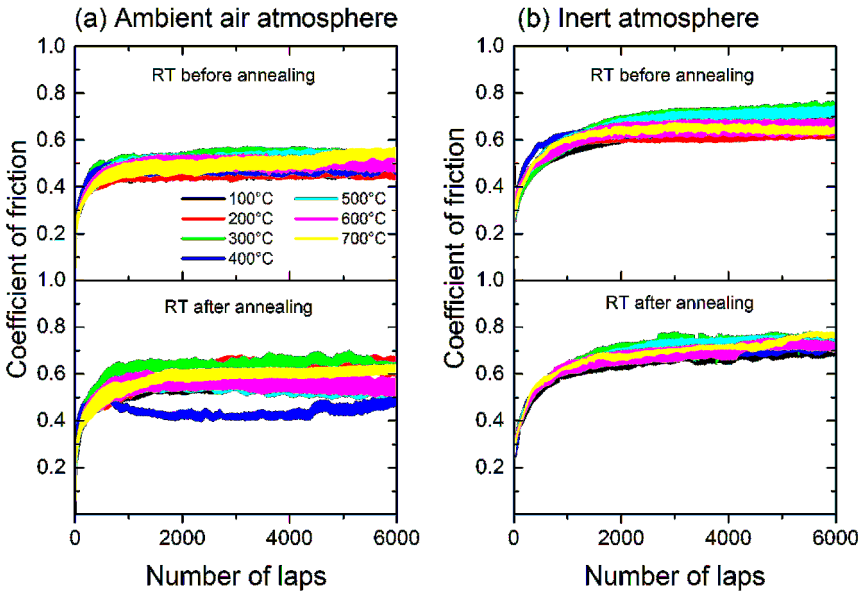

Figure 2.6: The evolution of COFs of CrAlN at RT (a) before and (b) after annealing to the temperature in the HT tribological tests in ambient air and inert atmosphere.

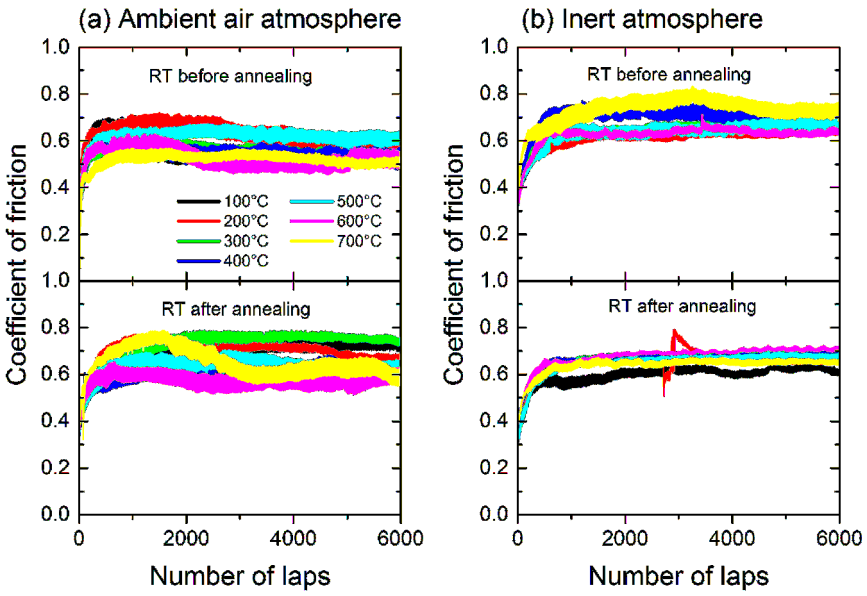

Figure 2.7: The evolution of COFs of CrAlSiN at RT (a) before and (b) after annealing to the temperature in the HT tribological tests in ambient air and inert atmosphere.

the wear coefficients in inert atmosphere were higher than in ambient air. The behavior is again most likely related to the adhesion problems encountered during the tests at these temperatures. The wear of the Al_2O_3 balls in inert atmosphere was analogous to the wear in ambient air atmosphere.

A wear coefficient below $1 \cdot 10^{-16} m^3 \cdot N^{-1} \cdot Lap^{-1}$ is considered as a low wear since no pronounced wear track could be observed on the coating surfaces in these cases. This means that for CrAlN significant coating wear was only observed in ambient air at 600 and 700 °C and between 400 and 700 °C in inert atmosphere. CrAlSiN was generally more wear resistant since

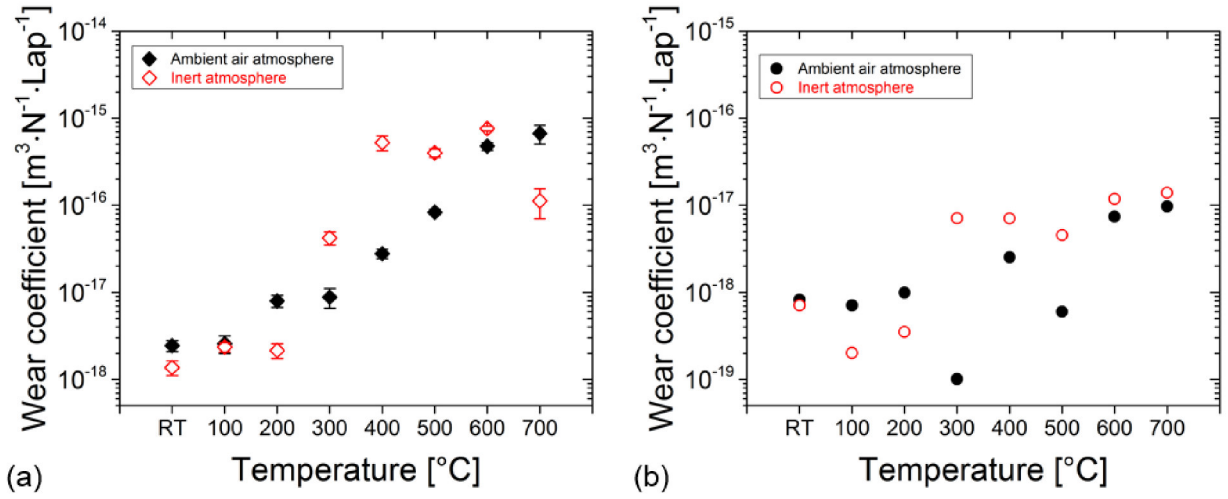

Figure 2.8: Wear coefficients of (a) the CrAlN coating and (b) the Al_2O_3 counterpart at temperatures from RT to 700 °C in ambient air and inert atmospheres.

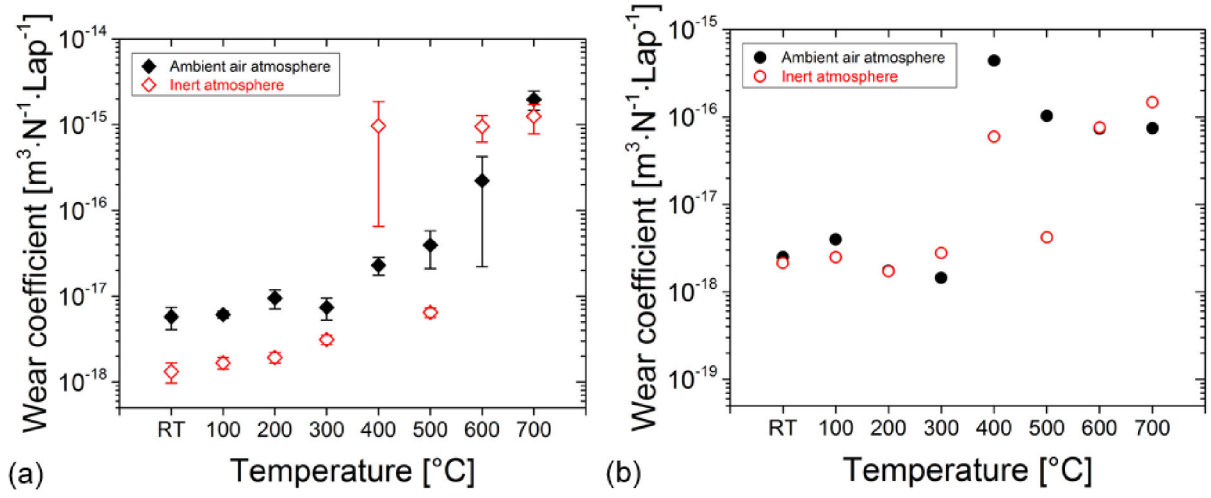

Figure 2.9: Wear coefficients of (a) the CrAlSiN coating and (b) the Al_2O_3 counterpart at temperatures from RT to 700 °C in ambient air and inert atmospheres.

the value of $1 \cdot 10^{-16} m^3 \cdot N^{-1} \cdot Lap^{-1}$ was only exceeded at 700 ℃ in both atmospheres excluding the above mentioned adhesion problems. The generally higher wear of the counterparts when tested against CrAlSiN than against CrAlN can be understood by the higher hardness of the former coating causing higher wear of the softer counterpart material.

Following the ball-on-disk tests, the wear track on the coatings and the wear scars of the counterparts were analyzed by Raman spectroscopy to identify possible changes of the coating during the exposure to high temperature and tribological wear contact. Raman spectra were taken from different positions in the coating wear tracks and counterpart wear scars after testing in ambient and inert atmosphere at temperatures from 300 to 700 ℃. In the case of CrAlN, no significant changes were observed from 300 to 500 ℃ in ambient air atmosphere, since the Raman spectra recorded on the worn surfaces were identical to the spectrum of the pristine coating. This indicates an undamaged coating after each test cycle and is in agreement with the measurements regarding the wear track depth (see Fig. 2.4). However, at 600 and 700 ℃ Fe oxides from the substrate, Cr oxide from the coating and Al oxide from either the counterpart or the coating were detected at different positions of the wear tracks due to intense wear of the coating during the tribological test.

A similar behavior was encountered in inert atmosphere, i.e. Fe, Al and Cr oxides were found at 600 and 700 ℃ which indicates that the established inert atmosphere was not sufficient to prevent oxidation completely or chemical reactions between between the Al_2O_3 counterpart and the coating occurred in the tribological contact zone. In addition the same oxides were also noticed at 400 and 500 ℃, which indicates that the coating was worn through at these temperatures. According to the 3D profiles of the wear tracks in Fig. 2.4, a narrow but deep segment of the steel substrate was exposed at 400 and 500 ℃, whereas at 600 and 700 ℃ the coating was more evenly worn-off during the test.

The Raman spectra for the CrAlSiN coatings in ambient air atmosphere showed an equal trend as the CrAlN coating in ambient air, since starting from 300 to 500 ℃ the Raman spectra at different positions were mainly identical to the pristine coating. Again, Fe, Al and Cr oxides were detected at 600 and 700 ℃ as a result of the partial removal of the coating and the exposure of the HSS substrate to the ambient environment. After tribological testing of CrAlSiN in inert atmosphere, oxides were identified in the wear tracks at 400 and 600 ℃. The appearance of the oxides at these temperatures is most likely related to the adhesion problems. At 700 ℃ some indications for the formation of oxides were also noticed, but less pronounced than in the case of CrAlN in inert atmosphere.

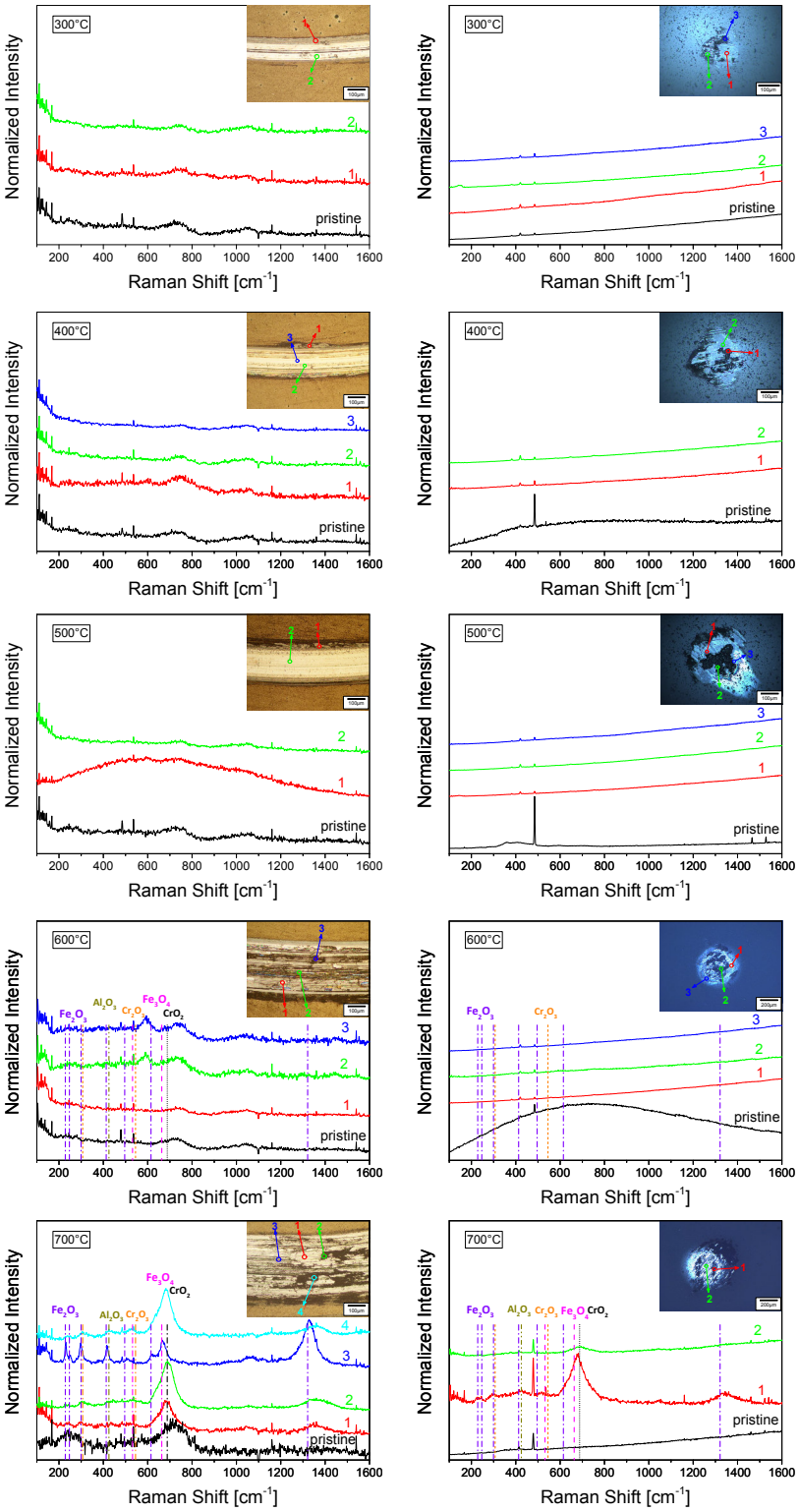

Figure 2.10: Raman spectra recorded at different positions on the CrAlN coating (left column) and the Al_2O_3 counterpart (right column) after tribological testing in ambient air atmosphere at elevated temperatures. Reference peak positions of Fe_2O_3, Al_2O_3, Cr_2O_3, Fe_3O_4 and CrO_2 are indicated.

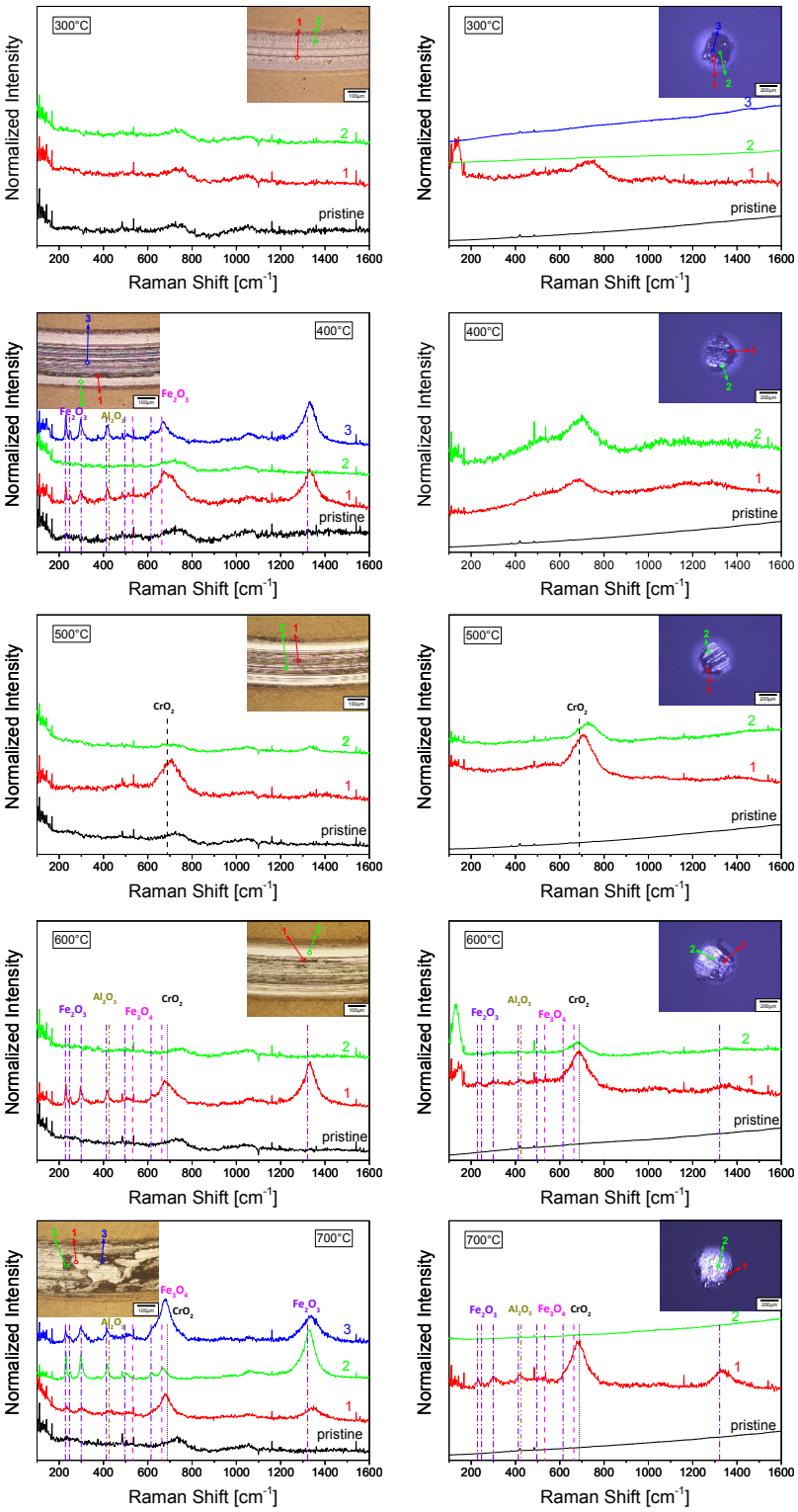

Figure 2.11: Raman spectra recorded at different positions on the CrAlN coating (left column) and the Al_2O_3 counterpart (right column) after tribological testing in inert atmosphere at elevated temperatures. Reference peak positions of Fe_2O_3, Al_2O_3, Fe_3O_4 and CrO_2 are indicated.

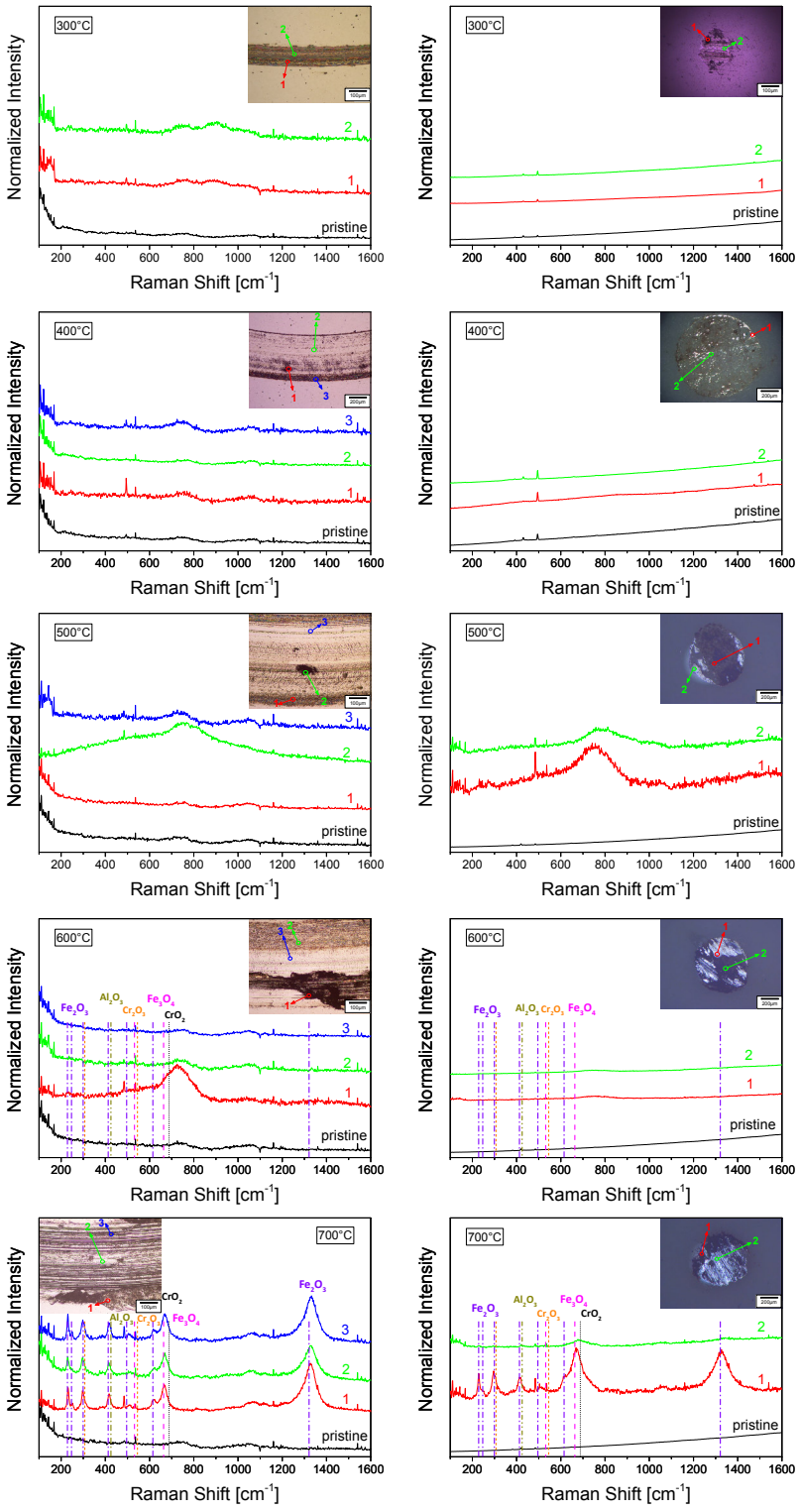

Figure 2.12: Raman spectra recorded at different positions on the CrAlSiN coating (left column) and the Al_2O_3 counterpart (right column) after tribological testing in ambient air atmosphere at elevated temperatures. Reference peak positions of Fe_2O_3, Al_2O_3, Cr_2O_3, Fe_3O_4 and CrO_2 are indicated.

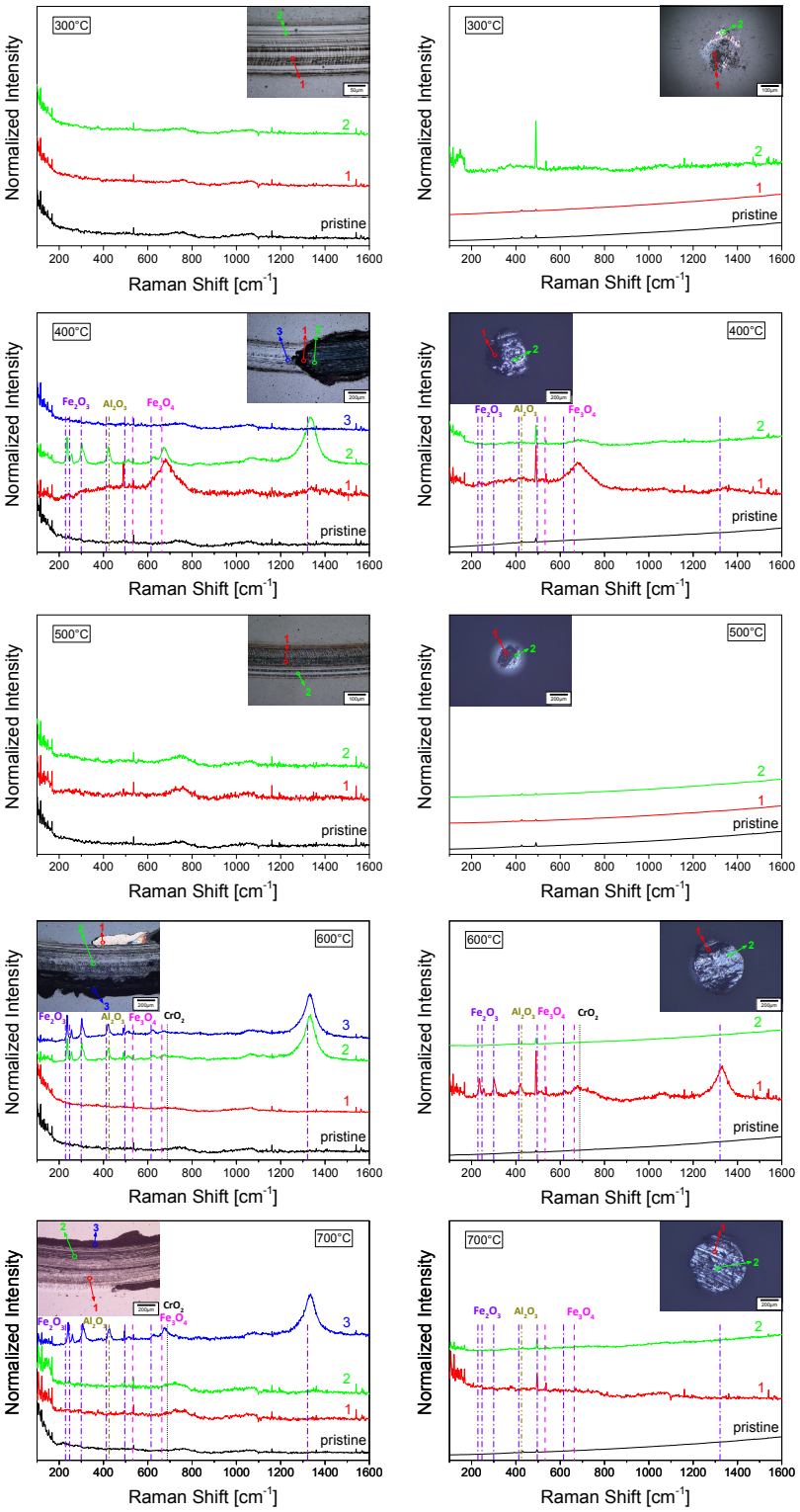

Figure 2.13: Raman spectra recorded at different positions on the CrAlSiN coating (left column) and the Al_2O_3 counterpart (right column) after tribological testing in inert atmosphere at elevated temperatures. Reference peak positions of Fe_2O_3, Al_2O_3, Fe_3O_4 and CrO_2 are indicated.

2.4 Summary and conclusions

CrAlN and CrAlSiN coatings deposited by magnetron sputtering were analyzed as to their tribological behavior at elevated temperatures. While the friction of both coatings was largely unaffected by changing the testing temperature and environment, i.e. ambient air and inert atmosphere, the wear of CrAlN at temperatures ranging from 400 to 600 ℃ was increased in the absence of oxygen. In the case of CrAlSiN, the wear in inert atmosphere showed the same increasing trend with rising temperature in both atmospheres, but the wear in inert atmosphere was generally slightly lower. Exceptions were caused by adhesion problems of the coating for individual tests. The performed Raman analysis of the wear tracks on the coatings and wear scars on the Al_2O_3 counterparts confirmed evolution of the wear of CrAlN and CrAlSiN with increasing temperature in the different atmospheres. The formation of the protective oxide layer on CrAlN at elevated temperatures was beneficial in terms of wear resistance, whereas the wear behavior of CrAlSiN was unaffected. The obtained results show the importance of studying the influence of the surrounding atmosphere on the wear behavior at elevated temperatures.

References

[1] H. Hasegawa, M. Kawate, T. Suzuki, Surface and Coatings Technology 200 (7) (2005) 2409–2413.

[2] A. Reiter, V. Derflinger, B. Hanselmann, T. Bachmann, B. Sartory, Surface and Coatings Technology 200 (7) (2005) 2114–2122.

[3] A. Kimura, M. Kawate, H. Hasegawa, T. Suzuki, Surface and Coatings Technology 169-170 (2003) 367–370.

[4] A. Sugishima, H. Kajioka, Y. Makino, Surface and Coatings Technology 97 (1997) 590–594.

[5] A. E. Reiter, C. Mitterer, B. Sartory, Journal of Vacuum Science and Technology A 25 (4) (2007) 711.

[6] J. L. Endrino, S. Palacín, M. H. Aguirre, A. Gutiérrez, F. Schaefers, Acta Materialia 55 (6) (2007) 2129–2135.

[7] C. Tritremmel, R. Daniel, M. Lechthaler, P. Polcik, C. Mitterer, Thin Solid Films 534 (2013) 403–409.

[8] W. Kalss, A. Reiter, V. Derflinger, C. Gey, J. L. Endrino, International Journal of Refractory Metals and Hard Materials 24 (5) (2006) 399–404.

[9] E. Spain, J. C. Avelar-Batista, M. Letch, J. Housden, B. Lerga, Surface and Coatings Technology 200 (5-6) (2005) 1507–1513.

[10] T. Polcar, A. Cavaleiro, Surface and Coatings Technology 206 (6) (2011) 1244–1251.

[11] T. Polcar, T. Vitu, J. Sondor, A. Cavaleiro, Plasma Processes and Polymers 6 (S1) (2009) 935–940.

[12] K. Holmberg, A. Matthews, Coatings Tribology: Properties, Mechanisms, Techniques and Applications in Surface Engineering, Elsevier, Amsterdam, Netherlands, 2009.

[13] N. Vidakis, A. Antoniadis, N. Bilalis, Journal of Materials Processing Technology 143-144 (1) (2003) 481–485.

[14] H.-R. Stock, A. Schultz, W. Ensinger, J. Güttler, E. Fromm, D. Müller, W. Busch, DIN Fachbericht 39 (1993) 210–234.

[15] W. Oliver, G. Pharr, Journal of Materials Research 7 (06) (1992) 1564–1583.

[16] E. Rabinowicz, Friction and Wear of Materials, John Wiley and Sons, New York, 1965.

[17] J. C. Sánchez-López, A. Contreras, S. Domínguez-Meister, A. García-Luis, M. Brizuela, Thin Solid Films 550 (2014) 413–420.

[18] H. C. Barshilia, K. Rajam, Journal of Materials Research 19 (11) (2011) 3196–3205.

[19] A. Öztürk, K. Ezirmik, K. Kazmanl, M. Ürgen, O. Erylmaz, A. Erdemir, Tribology International 41 (1) (2008) 49–59.

[20] S. Kikuchi, K. Kawauchi, M. Kurosawa, H. Honjho, T. Yagishita, Analytical Sciences 21 (3) (2005) 197–198.

[21] A. Misra, H. Bist, M. Navati, R. Thareja, J. Narayan, Materials Science and Engineering: B 79 (1) (2001) 49–54.

[22] M. Pfeiler, J. Zechner, M. Penoy, C. Michotte, C. Mitterer, M. Kathrein, Surface and Coatings Technology 203 (20-21) (2009) 3104–3110.

[23] A. E. Reiter, C. Mitterer, M. Rebelo de Figueiredo, R. Franz, Tribology Letters 37 (3) (2010) 605–611.

[24] A. Liu, J. Deng, H. Cui, Y. Chen, J. Zhao, International Journal of Refractory Metals and Hard Materials 31 (2012) 82–88.

[25] R. Franz, M. Lechthaler, P. Polcik, M. Rebelo de Figueiredo, C. Mitterer, Tribology Letters 45 (1) (2012) 143–152.

[26] J. Nohava, P. Dessarzin, P. Karvankova, M. Morstein, Tribology International 81 (2015) 231–239.